PHYSICAL REVIEW D **96,** 083508 (2017)

# Baryons still trace dark matter: Probing CMB lensing maps for hidden isocurvature

Tristan L. Smith,[1] Julian B. Muñoz,[2] Rhiannon Smith,[1] Kyle Yee,[1] and Daniel Grin[3]
[1]*Department of Physics and Astronomy, Swarthmore College, 500 College Avenue, Swarthmore, Pennsylvania 19081, United States*
[2]*Department of Physics and Astronomy, Johns Hopkins University, 3400 N. Charles Street, Baltimore, Maryland 21218, United States*
[3]*Department of Physics and Astronomy, Haverford College, 370 Lancaster Avenue, Haverford, Pennsylvania 19041, United States*
(Received 6 May 2017; published 11 October 2017)

Compensated isocurvature perturbations (CIPs) are primordial fluctuations that balance baryon and dark-matter isocurvature to leave the total matter density unperturbed. The effects of CIPs on the cosmic microwave background (CMB) anisotropies are similar to those produced by weak lensing of the CMB: smoothing of the power spectrum and generation of non-Gaussian features. Here, an entirely new CIP contribution to the standard estimator for the lensing-potential power spectrum is derived. *Planck* measurements of the temperature and polarization power spectrum, as well as estimates of CMB lensing, are used to place limits on the variance of the CIP fluctuations on CMB scales, $\Delta^2_{\rm rms}(R_{\rm CMB})$. The resulting constraint of $\Delta^2_{\rm rms}(R_{\rm CMB}) < 4.3 \times 10^{-3}$ at 95% confidence level (CL) using this new technique improves on past work by a factor of ∼3. We find that for *Planck* data our constraints almost reach the sensitivity of the optimal CIP estimator. The method presented here is currently the most sensitive probe of the amplitude of a scale-invariant CIP power spectrum, $A_{\rm CIP}$, placing an upper limit of $A_{\rm CIP} < 0.017$ at 95% CL. Future measurements of the large-scale CMB lensing-potential power spectrum could probe CIP amplitudes as low as $\Delta^2_{\rm rms}(R_{\rm CMB}) = 8 \times 10^{-5}$ at 95% CL (corresponding to $A_{\rm CIP} = 3.2 \times 10^{-4}$).

DOI: 10.1103/PhysRevD.96.083508

## I. INTRODUCTION

The standard cosmological model has been established using a wide range of observations: estimates of the primordial light element abundances predicted by standard big bang nucleosynthesis (BBN) [1,2], the observed isotropy and structure of the acoustic peaks in the cosmic microwave background (CMB) [3–7], increasingly restrictive upper limits to the level of non-Gaussianity in the CMB [8], the large-scale clustering of galaxies [9], and upper limits to nonstandard initial conditions [10,11]—just to name a few. In addition to these successes, there are some inconsistencies that have been pointed out, such as the current mismatch between supernovae and CMB determinations of the Hubble constant [12], a slight hemispherical power asymmetry in the CMB [13], tension between low-redshift weak lensing measurements from the CFHTLenS and CMB estimates of the current matter density, $\Omega_m$, and density fluctuations on 8 $h^{-1}$ Mpc scales, $\sigma_8$ [14]. These examples are not meant to be exhaustive but instead to make the point that it is by looking for deviations from the standard cosmological model that we increase our knowledge of, and focus our questions about, the physical nature of the universe.

In this work we search for compensated isocurvature perturbations (CIPs) using observations of the CMB made by the *Planck* satellite [15]. The standard cosmological model predicts that the initial perturbations in the early universe are adiabatic (i.e., isentropic). Several other types of initial perturbations may be established by nonstandard processes (such as axion physics [16], or alternatives to single-field slow-roll inflation such as the curvaton scenario [17–19]). The most general set of these nonstandard perturbations, called isocurvature perturbations, describe the "normal modes" of the early universe and as such evolve independently from each other and the standard adiabatic perturbations. Most previous studies have placed constraints on the amplitude of pure isocurvature modes, finding that their amplitude cannot be larger than a few percentage points of that of the standard adiabatic perturbations [11]. On the other hand, CIPs are not pure modes, but are instead composed of a linear combination of baryon and cold dark matter (CDM) isocurvature. The amplitudes of these two modes are set so as to leave the total matter perturbation unchanged. CIPs are only weakly constrained by current data since the effects of CIPs on scales $k \lesssim 200$ Mpc$^{-1}$ appear at second order in the CIP amplitude [20–22]. This makes the search for CIPs in current data sets, which probe scales $k \lesssim 10$ Mpc$^{-1}$, particularly challenging.

Previous studies have placed constraints on CIPs. A CIP leads to fluctuations of the baryon-to-dark-matter ratio which may be observed in the baryon fraction of galaxies [23] or in the detailed structure of the baryon acoustic

 

oscillations [24]. It also generically leads to fluctuations in the primordial light element abundances [23]. These effects can be used to place constraints on CIPs for a variety of length scales, from ∼1–100 Mpc.

In the CMB, CIPs cause a modulation of the photon-baryon sound speed leading to second-order effects in both the CMB power spectrum and trispectrum. Given that both CIPs and the weak lensing of the CMB higher-order effects [25], it is unsurprising that the mathematical expressions for their effect on the CMB are structurally similar. In particular, both cause smoothing of the small-scale CMB power spectrum [26,27], and generate a (non-Gaussian) connected CMB trispectrum [21,22].

An optimal estimator of CIPs using the CMB trispectrum was derived in Refs. [18,21,22]. To evaluate this estimator on the *Planck* data would be computationally intensive, requiring careful treatment of sky cuts and many simulations of mock CMB maps to obtain the relevant covariance matrices. Instead, in this work we note that the standard estimator for the lensing-potential power spectrum [28], already implemented in the publicly available data products from *Planck* [29], has sensitivity to the CIP field on large angular scales. We thus use current estimates of the lensing-potential power spectrum from *Planck* to search for CIPs and obtain limits to a scale-invariant CIP spectrum that are a factor of ∼3 better than the limit from the CMB power spectrum alone: the CIP variance on CMB scales is $\Delta^2_{\rm rms}(R_{\rm CMB}) \lesssim 4.3\times10^{-3}$ at 95% confidence level (CL). Using standard forecasting techniques, we find that we have extracted nearly all the information on CIPs that can be extracted from *Planck* maps. For a future nearly cosmic variance–limited experiment like the CMB Stage 4 (CMB-S4), we find that an optimal analysis of the full trispectrum improves on the lensing-potential + CMB power spectrum analysis by a factor of ∼4, driven mainly by polarization measurements.

Throughout this paper we use a fiducial cosmology that is spatially flat with parameters [7]: $\Omega_b h^2 = 0.0222$, $\Omega_c h^2 = 0.1203$, $\Omega_\nu h^2 = 0.00064$ (corresponding to two massless neutrinos and one massive neutrino with $m = 0.06\,\text{eV}$), $H_0 = 67.12\,\text{km}\,\text{s}^{-1}\,\text{Mpc}^{-1}$, $A_s = 2.09\times10^{-9}$, $n_s = 0.96$, and $\tau = 0.065$. We begin with a summary of the physics of compensated isocurvature perturbations in Sec. II, and then review the effects of CIPs on the observed CMB fluctuations in Sec. III. Previous constraints to CIPs are summarized and explained in Sec. IV. Our new CIP constraints, using a combination of the observed *Planck* lensing potential and CMB primary spectra, are presented in Sec. V. We discuss the promise of more optimal estimators and future experiments in Sec. VI, and conclude in Sec. VII. We also include several appendices that present the details of our calculations.

## II. COMPENSATED ISOCURVATURE PERTURBATIONS

Solutions to the linearized Einstein and Boltzmann equations, which describe perturbations to an otherwise isotropic and homogeneous universe, can be divided up into a set of normal modes, each of which evolve independently (see, e.g., Ref. [30]). For example, a given Fourier mode of the density contrast ($\delta_i \equiv \delta\rho_i/\bar{\rho}_i$) of a species $i$ can be written as

$$\begin{aligned}\delta_i(\vec{k},\tau) &= \sum_n \xi_n(\vec{k}) A_n T_i^n(k,\tau),\\ &= \delta_i^{\rm ad} + \delta_i^{\rm b,iso} + \delta_i^{\rm c,iso} + \cdots,\end{aligned} \tag{1}$$

where $n$ denotes the type of initial conditions (i.e., adiabatic would be $n = 0$, baryon isocurvature $n = 1$, and so forth), $A_n$ gives the relative amplitude of the modes, $\xi_n(\vec{k})$ is a stochastic amplitude with zero mean, and $T_i^n(k,\tau)$ is the transfer function for each species and each type of initial condition. As is standard, we further assume that $\xi_n(\vec{k})$ is pulled from a Gaussian probability distribution and is statistically isotropic with some primordial power spectrum, $\langle \xi_n(\vec{k}) \xi^*_{n'}(\vec{k}')\rangle = (2\pi)^3 P_{nn'}(k)\delta_D^{(3)}(\vec{k}-\vec{k}')$. Similar equations can be written for the other perturbed moments of the stress-energy tensor of each species. The linearized Einstein and Boltzmann equations determine the behavior of the transfer functions $T_i^n(k,\tau)$.

For any set of initial conditions the relative entropy perturbation between any species and photons is given by

$$S_i \equiv 3(\zeta_i - \zeta_\gamma) = -3\mathcal{H}\left(\frac{\delta\rho_i}{\rho_i'} - \frac{\delta\rho_\gamma}{\rho_\gamma'}\right), \tag{2}$$

where $\zeta_i$ is the curvature perturbation in a gauge where that species, $i$, is uniform, $\mathcal{H} \equiv a'/a$, and the prime indicates a derivative with respect to conformal time, $\tau$. We can simplify this expression by noting that the continuity equation applied to the background density is

$$\rho_i' = -3\mathcal{H}\rho_i(1+w_i), \tag{3}$$

so

$$S_i = \frac{1}{1+w_i}\delta_i - \frac{3}{4}\delta_\gamma. \tag{4}$$

We consider a universe filled with photons ($\gamma$), neutrinos ($\nu$), baryons ($b$), and cold dark matter ($c$) (we also consider a cosmological constant, $\Lambda$, which does not cluster). The *total* matter ($m$) is the sum of the baryons and CDM. The standard adiabatic initial conditions have $S_i = 0$ for all species; initial conditions which have $S_i \neq 0$ for some species, as well as leave the Ricci scalar curvature of the universe unperturbed, are called isocurvature perturbations and are set independently of the adiabatic mode [31–33].

A compensated isocurvature perturbation is a linear combination of baryon and CDM isocurvature which has $S_\nu = S_m = 0$. The evolution of the perturbations is

then determined by the initial values of the linear combinations [33]

$$\delta_\gamma = \delta_\gamma^{\rm ad}, \tag{5}$$

$$\delta_\nu = \delta_\nu^{\rm ad}, \tag{6}$$

$$\delta_c = \delta_c^{\rm ad} + \delta_c^{\rm CIP}, \tag{7}$$

$$\delta_b = \delta_b^{\rm ad} + \delta_b^{\rm CIP}, \tag{8}$$

$$\delta_m = R_b\delta_b + R_c\delta_c = \delta_m^{\rm ad}, \tag{9}$$

where

$$R_c \equiv \frac{\rho_c}{\rho_c + \rho_b}, \tag{10}$$

$$R_b \equiv \frac{\rho_b}{\rho_c + \rho_b}. \tag{11}$$

As first pointed out in Ref. [20] on scales larger than the baryon sound horizon, $k \lesssim 200\ {\rm Mpc}^{-1}$, the CIP modes do not evolve in time and can be treated as a function of position only. On these scales, we define the stochastic CIP field as $\Delta(\vec{k}) \equiv \delta_b^{\rm CIP}(\vec{k})$ so that $\delta_c^{\rm CIP}(\vec{k}) = -\Delta(\vec{k})\Omega_b/\Omega_c$. Since the CIP modes do not evolve in time, the baryon and CDM densities are spatially modulated by $\Delta$ as follows:

$$\rho_b(\vec{x}) = \bar{\rho}_b[1 + \Delta(\vec{x})], \tag{12}$$

$$\rho_c(\vec{x}) = \bar{\rho}_c\left[1 - \frac{\bar{\rho}_b}{\bar{\rho}_c}\Delta(\vec{x})\right], \tag{13}$$

where $\bar{\rho}_b/\bar{\rho}_c = \bar{\Omega}_b/\bar{\Omega}_c \simeq 0.2$ is the unperturbed (homogeneous) ratio of the baryon to cold dark matter density.

The CIP field can have an arbitrary correlation with the primordial curvature perturbation [18,20]. Most of the previous work on CIPs has assumed $\Delta$ is uncorrelated with the primordial curvature perturbation (e.g., Refs. [21,22,26,34]). This assumption greatly simplifies the effects of a CIP since in this case only autocorrelations of $\Delta$ are nonzero. On the other hand, fully correlated CIPs are a natural prediction of the curvaton scenario [18,19]. The additional correlations present in this case lead to a greater sensitivity to the CIP field [18,35], and in future work we will leverage this sensitivity to obtain forecasts and constraints to curvaton-inspired CIPs. For the rest of this paper, we consider only CIPs which are uncorrelated with the primordial curvature perturbation.

## III. CIPS AND THE CMB

The main effect of CIPs on the CMB is the spatial modulation in the photon/baryon sound speed [18]. In particular, in the presence of a CIP the acoustic waves that generate the structure of the observed CMB anisotropies propagate through an inhomogeneous medium with a sound speed that varies as

$$c_s^2(\vec{x}) = \frac{1}{3}\left(1 + \frac{3}{4}\frac{\bar{\rho}_b[1 + \Delta(\vec{x})]}{\bar{\rho}_\gamma}\right)^{-1}, \simeq (\bar{c}_s)^2\left[1 - \frac{3\bar{\rho}_b}{3\bar{\rho}_b + 4\bar{\rho}_\gamma}\Delta(\vec{x})\right]. \tag{14}$$

Additionally, the modulation of $\rho_b$ leads to a spatial variation in the visibility function at decoupling. For CIP scales smaller than the acoustic horizon at decoupling ($L \gtrsim 100$), the effects of the CIP modulation are suppressed [18], and so we only include CIP multipoles at scales larger than the acoustic horizon. Writing the Fourier transform of the CIP field as

$$\Delta(\vec{x}) = \int \frac{d^3k}{(2\pi)^3}\Delta(\vec{k})e^{i\vec{k}\cdot\vec{x}}, \tag{15}$$

its power spectrum is given by

$$\langle\Delta(\vec{k})\Delta^*(\vec{k}')\rangle = (2\pi)^3\delta_D^{(3)}(\vec{k} - \vec{k}')P_{\Delta\Delta}(k), \tag{16}$$

and we can compute the CIP variance over some length scale $R$ as

$$\Delta^2_{\rm rms}(R) = \frac{1}{2\pi^2}\int k^2dk[3j_1(kR)/(kR)]^2P_{\Delta\Delta}(k), \tag{17}$$

assuming a spherical top-hat window function (of radius $R$) for density fluctuations in real space. Finally, the CIP angular distribution at the last-scattering surface will be given by

$$\Delta_{LM} = \frac{4\pi i^L}{(2\pi)^{3/2}}\int d^3k\Delta(\vec{k})j_L(k\chi_*)Y^*_{LM}(\hat{k}), \tag{18}$$

which gives rise to an angular power spectrum

$$C_L^{\Delta\Delta} = \langle\Delta_{LM}\Delta^*_{LM}\rangle = \frac{2}{\pi}\int k^2dkP_{\Delta\Delta}(k)j_L^2(k\chi_*), = \frac{A_{\rm CIP}}{\pi L(L+1)} \tag{19}$$

if we assume that the CIP power spectrum is scale invariant: $P_{\Delta\Delta}(k) = A_{\rm CIP}/k^3$. This allows us to write

$$\Delta^2_{\rm rms}(R_{\rm CMB}) = \sum_{L=1}^{100}\frac{2L+1}{4\pi}C_L^{\Delta\Delta} \simeq \frac{A_{\rm CIP}}{4}, \tag{20}$$

where we have truncated the sum at $L = 100$ since, as stated before, the CIP modulation damps away on scales

smaller than the acoustic horizon at decoupling. Finally, we find the expression

$$C_L^{\Delta\Delta} \simeq \frac{4}{\pi}\frac{\Delta^2_{\rm rms}(R_{\rm CMB})}{L(L+1)}. \tag{21}$$

The effects of a CIP modulation on the anisotropies of the CMB are most clearly understood using a flat-sky approximation. For the discussion here we only present results for the temperature anisotropies. When searching for CIPs, we use both temperature and polarization with the full-sky expressions found in Appendix B.

Weak gravitational lensing and CIPs can be thought of as a modulation of a "background" CMB anisotropy $T(\hat{n})$ yielding an observed anisotropy $T_{\rm obs}(\hat{n})$. In the presence of both weak gravitational lensing and CIPs the temperature anisotropies are given by

$$\begin{aligned} T_{\rm obs}(\hat{n}) &= T[\hat{n}+\vec{\nabla}\phi(\hat{n}), \Delta(\hat{n})], \\ &\simeq T(\hat{n}) + \nabla_i\phi\nabla^i T + \Delta(\hat{n})\frac{\partial T}{\partial\Delta}(\hat{n})\Big|_{\Delta=0} \\ &\quad + \frac{1}{2}\left(\nabla_i\phi\nabla_j\phi\nabla^i\nabla^j T + \Delta^2(\hat{n})\frac{\partial^2 T}{\partial\Delta^2}(\hat{n})|_{\Delta=0}\right) + \cdots, \end{aligned} \tag{22}$$

where the terms proportional to derivatives of $\phi(\hat{n})$ are standard lensing contributions as first derived in Refs. [36,37] and described in Ref. [38]. Additionally, one must include a noise term, so then the total observed temperature at each point on the sky can be written $T^t(\hat{n}) = T_{\rm obs}(\hat{n}) + T^N(\hat{n})$, where we assume that we are using beam-deconvolved maps. This leads to an estimated power spectrum for the beam-deconvolved map

$$C_l^{TT,\rm t} = C_l^{TT,\rm obs} + C_l^{TT,N}, \tag{23}$$

where the inverse variance–weighted sum over all channels $i$ gives

$$C_l^{TT,N} = \left(\sum\nolimits_i w_{T,i}^{-2} e^{-l^2\sigma^2_{b,i}}\right)^{-1}, \tag{24}$$

where $\sigma_{b,i} \equiv \theta_i/\sqrt{8\ln 2}$, $\theta_i$ is the full-width half-maximum, and $w_{T,i}$ is the weight per solid angle for each channel.

Taking the Fourier transform of the temperature map we have

$$\begin{aligned} T_{\rm obs}(\vec{l}) &\equiv \int d^2\hat{n} T_{\rm obs}(\hat{n}) e^{-i\vec{l}\cdot\hat{n}}, \\ &= T(\vec{l}) + \delta T^{(1)}(\vec{l}) + \delta T^{(2)}(\vec{l}), \end{aligned} \tag{25}$$

where the first- and second-order terms are given by

$$\begin{aligned} \delta T^{(1)}(\vec{l}) &= \int \frac{d^2 l'}{(2\pi)^2} T(\vec{l}')\phi(\vec{l}-\vec{l}') L_\phi^{(1)}(\vec{l},\vec{l}') \\ &\quad + \frac{\partial T(\vec{l}')}{\partial\Delta}\Big|_{\Delta=0}\Delta(\vec{l}-\vec{l}'), \end{aligned} \tag{26}$$

$$\begin{aligned} \delta T^{(2)}(\vec{l}) &= \frac{1}{2}\int \frac{d^2 l'}{(2\pi)^2}\frac{d^2 l''}{(2\pi)^2} T(\vec{l}')\phi(\vec{l}'') \\ &\quad \times \phi(\vec{l}-\vec{l}'-\vec{l}'') L_\phi^{(2)}(\vec{l},\vec{l}',\vec{l}'') \\ &\quad + \frac{\partial^2 T(\vec{l}')}{\partial\Delta^2}\Big|_{\Delta=0}\Delta(\vec{l}'')\Delta(\vec{l}-\vec{l}'-\vec{l}''), \end{aligned} \tag{27}$$

and for simpler notation we define

$$L_\phi^{(1)}(\vec{l},\vec{l}') \equiv -[(\vec{l}-\vec{l}')\cdot\vec{l}'], \tag{28}$$

$$L_\phi^{(2)}(\vec{l},\vec{l}',\vec{l}'') \equiv -[\vec{l}''\cdot\vec{l}'][(\vec{l}''+\vec{l}'-\vec{l})\cdot\vec{l}']. \tag{29}$$

The observed power spectrum is found by

$$\langle T_{\rm obs}(\vec{l}) T_{\rm obs}(\vec{l}')\rangle \equiv (2\pi)^2\delta_D^{(2)}(\vec{l}+\vec{l}') C_l^{TT,\rm obs}. \tag{30}$$

From these expressions it is straightforward to show that in the presence of both lensing and a CIP the observed power spectrum becomes

$$\begin{aligned} C_l^{TT,\rm obs} &= \tilde{C}_l^{TT}\left[1 - \int\frac{d^2L}{(2\pi)^2} C_L^{\phi\phi}(\vec{L}\cdot\vec{l})^2\right] \\ &\quad + \int\frac{d^2L}{(2\pi)^2}\tilde{C}^{TT}_{|\vec{l}-\vec{L}|} C_L^{\phi\phi}[(\vec{l}-L)\cdot\vec{L}]^2 \\ &\quad + \int\frac{d^2L}{(2\pi)^2} C^{dT,dT}_{|\vec{l}-\vec{L}|} C_L^{\Delta\Delta} \\ &\quad + C_l^{T,d^2T}\int\frac{d^2L}{(2\pi)^2} C_L^{\Delta\Delta}, \end{aligned} \tag{31}$$

$$\equiv \tilde{C}_l^{TT} + \delta C_l^{TT,\phi} + \delta C_l^{TT,\Delta}, \tag{32}$$

where $\tilde{C}_l^{TT}$ is the primordial CMB temperature power spectrum (without the CIP modulation and gravitational lensing) and we have defined

$$\langle\phi(\vec{l})\phi(\vec{l}')\rangle \equiv (2\pi)^2 C_l^{\phi\phi}\delta_D^{(2)}(\vec{l}+\vec{l}'), \tag{33}$$

$$\left\langle\frac{\partial T(\vec{l})}{\partial\Delta}\frac{\partial T(\vec{l}')}{\partial\Delta}\right\rangle \equiv (2\pi)^2 C_l^{dT,dT}\delta_D^{(2)}(\vec{l}+\vec{l}'), \tag{34}$$

$$\left\langle T(\vec{l})\frac{\partial^2 T(\vec{l}')}{\partial\Delta^2}\right\rangle \equiv (2\pi)^2 C_l^{T,d^2T}\delta_D^{(2)}(\vec{l}+\vec{l}'), \tag{35}$$

$$\delta C_l^{TT,\phi} \equiv \int \frac{d^2L}{(2\pi)^2} \tilde{C}^{TT}_{|\vec{l}-\vec{L}|} C_L^{\phi\phi} [(\vec{l}-L)\cdot\vec{L}]^2 - \tilde{C}_l^{TT} \int \frac{d^2L}{(2\pi)^2} C_L^{\phi\phi} (\vec{L}\cdot\vec{l})^2 \tag{36}$$

$$\delta C_l^{TT,\Delta} \equiv \int \frac{d^2L}{(2\pi)^2} C^{dT,dT}_{|\vec{l}-\vec{L}|} C_L^{\Delta\Delta} + C_l^{T,d^2T} \int \frac{d^2L}{(2\pi)^2} C_L^{\Delta\Delta}. \tag{37}$$

Since the CIP field modulates the baryon density, it follows that $C_l^{dT,dT}$ is only significant on scales smaller than the acoustic horizon, $l \gtrsim 100$. Furthermore, for a scale-invariant power spectrum $C_L^{\Delta\Delta} \propto 1/L^2$, which peaks at small $L$. This separation in scales allows us to write the CIP contribution to the observed CMB power spectrum as

$$\delta C_l^{TT,\Delta} \simeq \frac{1}{2} \Delta^2_{\rm rms}(R_{\rm CMB}) \frac{\partial^2 C_l^{TT}}{\partial \Delta^2}\bigg|_{\Delta=0}, \tag{38}$$

where in the flat-sky approximation $\Delta^2_{\rm rms}(R_{\rm CMB}) \equiv \int_1^{100} d^2L/(2\pi) C_L^{\Delta\Delta}$. The last approximation is still good for the full-sky expressions, as discussed in Appendix B.

Both weak lensing and the CIP modulation cause a smoothing of the CMB power spectra on scales smaller than the acoustic horizon [26]. We show the residual of the fiducial ΛCDM power spectrum with the CIP-modulated CMB power spectra, $\Delta\mathcal{D}_l^{XX'} \equiv l(l+1)\Delta C_l^{XX'}/(2\pi)$ with $X = \{T, E\}$, along with the *Planck* measurements in Fig. 1. This figure makes it clear how the measurements of the CMB power spectrum are sensitive to the presence of a CIP mode. In the residuals the additional smoothing of the peaks leads to an oscillatory structure, which is most apparent in the temperature power spectrum.

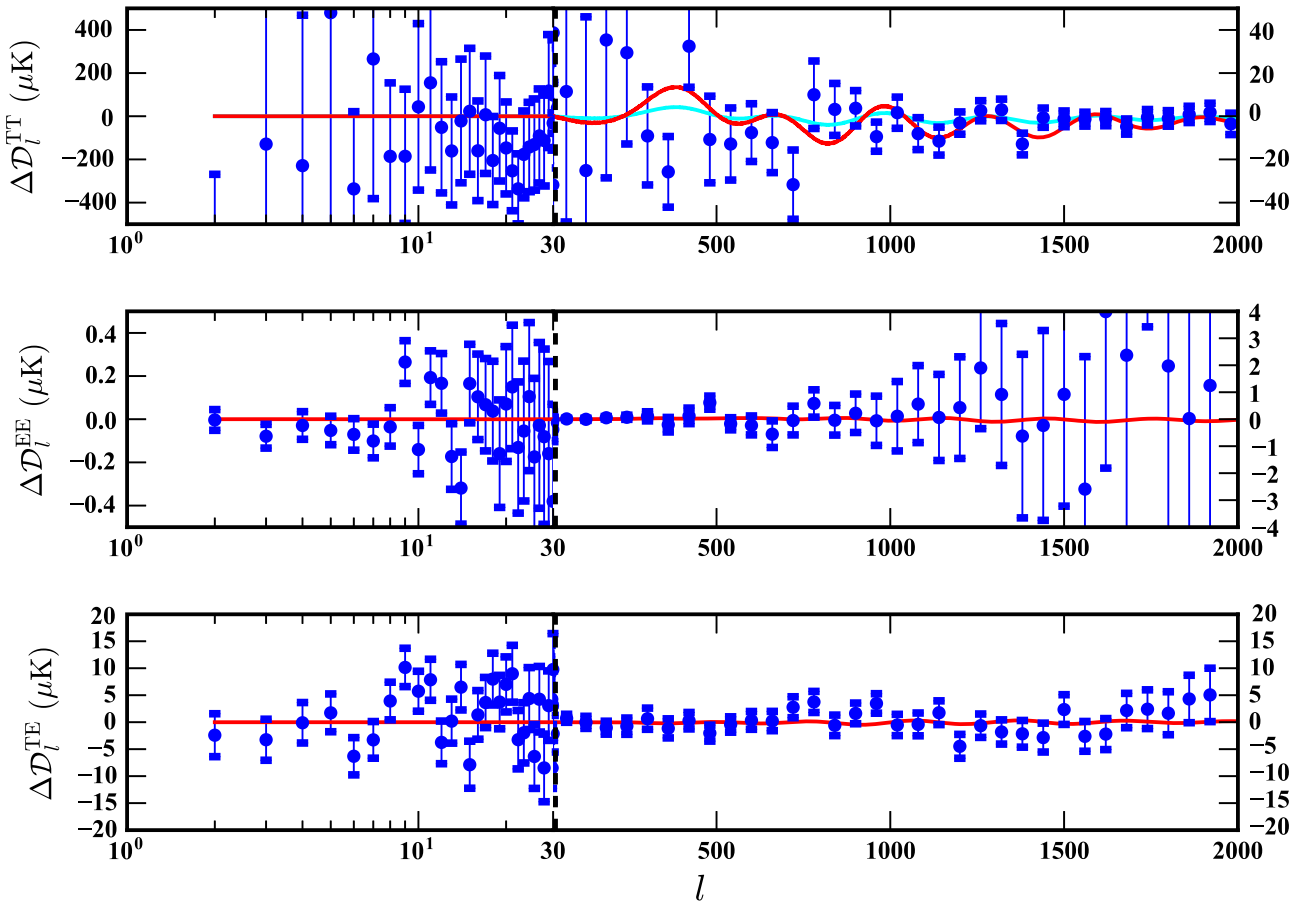


FIG. 1. A comparison between the difference between the standard ΛCDM CMB power spectra and one which has been modulated by a CIP mode. Each panel shows the binned residuals $\Delta\mathcal{D}_l^{XX'} \equiv l(l+1)\Delta C_l^{XX'}/(2\pi)$ from the *Planck* satellite (see Ref. [7] for details on the binning procedure). Two CIP-mode amplitudes are shown: the red curve shows the CIP mode which saturates the 95% CL upper limit using both the *Planck* measurements of the temperature and polarization CMB power spectra, $\Delta^2_{\rm rms}(R_{\rm CMB}) = 1.4 \times 10^{-2}$; the cyan curve (only visible in the top panel) shows the CIP mode which saturates the 95% CL upper limit using both the *Planck* measurements of the CMB power spectra as well as the lensing-potential power spectrum, $\Delta^2_{\rm rms}(R_{\rm CMB}) = 4.3 \times 10^{-3}$. Note that the horizontal scale is logarithmic up to $l = 29$ and then is linear; the vertical scale on the left- and right-hand sides are different.

The CIP modulation also produces a contribution to correlations beyond the CMB power spectrum. In particular, Refs. [18,21,22,34] construct an optimal estimator for $\Delta_{LM}$ from the connected part of the CMB four-point correlation, the trispectrum. The analysis of the CMB trispectrum is far from trivial, so here we utilize the fact that estimates of the lensing-potential power spectrum, $\phi$, are also built out of the connected part of the CMB trispectrum [28,29,39]. In the presence of CIPs, the estimator used to reconstruct the lensing-potential power spectrum gains an additional contribution proportional to $\Delta^2_{\rm rms}(R_{\rm CMB})$.

Both weak gravitational lensing and CIPs introduce a non-Gaussian connected trispectrum

$$\langle T(\vec{l}_1)T(\vec{l}_2)T(\vec{l}_3)T(\vec{l}_4)\rangle_c = \mathcal{T}(\vec{l}_1,\vec{l}_2,\vec{l}_3,\vec{l}_4)\delta^{(2)}(\vec{l}_1+\vec{l}_2+\vec{l}_3+\vec{l}_4). \quad (39)$$

The dominant contributions to the connected trispectrum are given by [40]

$$\begin{aligned}\mathcal{T}(\vec{l}_1,\vec{l}_2,\vec{l}_3,\vec{l}_4) \simeq\ & C^{\phi\phi}_{|\vec{l}_1+\vec{l}_2|} f_{TT}(\vec{l}_1,\vec{l}_2) f_{TT}(\vec{l}_3,\vec{l}_4) + C^{\Delta\Delta}_{|\vec{l}_1+\vec{l}_2|} h_{TT}(\vec{l}_1,\vec{l}_2) h_{TT}(\vec{l}_3,\vec{l}_4) \\ & + C^{\phi\phi}_{|\vec{l}_1+\vec{l}_3|} f_{TT}(\vec{l}_1,\vec{l}_3) f_{TT}(\vec{l}_2,\vec{l}_4) + C^{\Delta\Delta}_{|\vec{l}_1+\vec{l}_3|} h_{TT}(\vec{l}_1,\vec{l}_3) h_{TT}(\vec{l}_2,\vec{l}_4) \\ & + C^{\phi\phi}_{|\vec{l}_1+\vec{l}_4|} f_{TT}(\vec{l}_1,\vec{l}_4) f_{TT}(\vec{l}_2,\vec{l}_3) + C^{\Delta\Delta}_{|\vec{l}_1+\vec{l}_4|} h_{TT}(\vec{l}_1,\vec{l}_4) h_{TT}(\vec{l}_2,\vec{l}_3), \end{aligned} \quad (40)$$

where the lensing and CIP $TT$ response functions are given, respectively, by

$$f_{TT}(\vec{l}_1,\vec{l}_2) \equiv [(\vec{l}_1+\vec{l}_2)\cdot\vec{l}_1]\tilde{C}^{TT}_{l_1} + [(\vec{l}_1+\vec{l}_2)\cdot\vec{l}_2]\tilde{C}^{TT}_{l_2}, \quad (41)$$

$$h_{TT}(\vec{l}_1,\vec{l}_2) \equiv C^{T,dT}_{l_1} + C^{T,dT}_{l_2}, \quad (42)$$

and we have defined $C^{T,dT}_l$ through the correlation

$$\left\langle T(\vec{l})\frac{\partial T(\vec{l}')}{\partial\Delta}\right\rangle \equiv (2\pi)^2 C^{T,dT}_l \delta^{(2)}_D(\vec{l}+\vec{l}'). \quad (43)$$

Related expressions for the other correlated CMB maps using the flat-sky approximation are given in Appendix A.

We can construct an estimator for the lensing-potential power spectrum, $C^{\phi\phi}_L$, out of the four-point correlation function of the temperature, E- and B-mode polarization of the CMB. A nearly optimal, inverse variance–weighted, estimator has been derived in Ref. [28] and applied to the *Planck* CMB maps in Ref. [29]. As shown in Eq. (40), in the presence of a CIP modulation this estimator includes contributions from the CIP field.

In the flat-sky approximation, a minimum-variance estimator for the weak-lensing deflection field, $d(\vec{L}) \equiv L\phi(\vec{L})$ can be built out of off-diagonal correlations of the CMB temperature fluctuations, and is given by [28,29,41]

$$\hat{d}_{TT}(\vec{L}) \equiv \frac{A_{TT}(L)}{L}\int\frac{d^2l_1}{(2\pi)^2} T(\vec{l}_1)T(\vec{l}_2)F_{TT}(\vec{l}_1,\vec{l}_2), \quad (44)$$

where

$$\vec{l}_2 \equiv \vec{L} - \vec{l}_1, \quad (45)$$

$$F_{TT}(\vec{l}_1,\vec{l}_2) \equiv \frac{f_{TT}(\vec{l}_1,\vec{l}_2)}{2C^{TT,\rm t}_{l_1}C^{TT,\rm t}_{l_2}}, \quad (46)$$

$$A_{TT}(L) \equiv L^2\left[\int\frac{d^2l_1}{(2\pi)^2} f_{TT}(\vec{l}_1,\vec{l}_2)F_{TT}(\vec{l}_1,\vec{l}_2)\right]^{-1}. \quad (47)$$

The lensing-potential power spectrum is estimated from the power spectrum of the deflection field estimator in Eq. (44),

$$\hat{C}^{\phi\phi}_L \equiv \frac{1}{2\pi}\int_0^{2\pi}\frac{\hat{d}_{TT}(\vec{L})\hat{d}^*_{TT}(\vec{L})}{L^2}d\varphi_{\vec{L}} - B(L), \quad (48)$$

where $\varphi_{\vec{L}}$ is the angular coordinate of $\vec{L}$ and $B(L)$ (the bias) is a sum of the standard Gaussian and non-Gaussian contributions to the full four-point correlation [29,39,40]. Given that the estimator is inverse variance–weighted, the Gaussian variance is given by its normalization [41],

$$N^{(0)}_{TT,TT}(L) = A_{TT}(L). \quad (49)$$

In addition to this, Ref. [40] showed that there is a "non-Gaussian" bias, $N^{(1)}_{TT,TT}(L)$, arising from additional correlations between the lensing potential when computing the expectation value of Eq. (48).

In the presence of a CIP modulation, the expectation value of Eq. (48) gains another, CIP-induced, bias,

$$\langle\hat{C}^{\phi\phi}_L\rangle = C^{\phi\phi}_L + C^{\Delta\Delta}_L[Q^{TT}(L)]^2 + N^{(0)\rm CIP}_{TT,TT}(L)/L^2 + N^{(1)\rm CIP}_{TT,TT}(L)/L^2, \quad (50)$$

where the last two terms are the CIP-induced Gaussian and non-Gaussian bias, and

$$Q^{TT}(L) \equiv \frac{\int \frac{d^2l_1}{(2\pi)^2} h_{TT}(\vec{l}_1,\vec{l}_2)F_{TT}(\vec{l}_1,\vec{l}_2)}{\int \frac{d^2l_1}{(2\pi)^2} f_{TT}(\vec{l}_1,\vec{l}_2)F_{TT}(\vec{l}_1,\vec{l}_2)}. \quad (51)$$

The factors of $L^{-2}$ in Eq. (50) arise due to the conversion from the deflection field to the lensing potential [40]. Since the total temperature power spectrum has a CIP contribution given in Eq. (38), the CIP field contributes to the Gaussian bias of the standard estimator. In addition to this, along with the deflection field, the CIP field generates a non-Gaussian bias [40]. We compute the CIP non-Gaussian bias by replacing $f_{\Theta\Theta}$ with $h_{TT}$ [Eq. (42)] and $C_l^{\phi\phi}$ with $C_l^{\Delta\Delta}$ in Eq. (25) of Ref. [40]. These biases are, to leading order in the CIP amplitude,

$$N^{(0)\mathrm{CIP}}_{TT,TT}(L) = \frac{1}{2}\Delta^2_{\mathrm{rms}}(R_{\mathrm{CMB}})\left(\frac{A_{TT}(L)|_{\Delta^2_{\mathrm{rms}}=0}}{L^2}\right)^2 \int \frac{d^2l_1}{(2\pi)^2} f^2_{TT}(\vec{l}_1,\vec{l}_2)\left[\frac{1}{C^{TT}_{l_1}|_{\Delta^2_{\mathrm{rms}}=0}}\frac{\partial^2 C^{TT}_{l_1}}{\partial\Delta^2} + \frac{1}{C^{TT}_{l_2}|_{\Delta^2_{\mathrm{rms}}=0}}\frac{\partial^2 C^{TT}_{l_2}}{\partial\Delta^2}\right], \quad (52)$$

$$N^{(1)\mathrm{CIP}}_{TT,TT}(L) = \frac{A^2_{TT}(L)}{L^2}\int \frac{d^2l_1}{(2\pi)^2}\frac{d^2l_1'}{(2\pi)^2} F_{TT}(\vec{l}_1,\vec{l}_2)F_{TT}(\vec{l}_1{}',\vec{l}_2{}')[C^{\Delta\Delta}_{|\vec{l}_1-\vec{l}_1{}'|}h_{TT}(-\vec{l}_1,\vec{l}_1{}')h_{TT}(-\vec{l}_2,\vec{l}_2{}') + C^{\Delta\Delta}_{|\vec{l}_1-\vec{l}_2{}'|}h_{TT}(-\vec{l}_1,\vec{l}_2{}')h_{TT}(-\vec{l}_2,\vec{l}_1{}')]. \quad (53)$$

In practice, the *Planck* lensing analysis uses a combination of observed and simulated CMB maps to subtract off the Gaussian bias [29]. Since the simulated maps do not include a CIP contribution, some fraction of the CIP contribution to the Gaussian bias may not be fully subtracted. Additionally, the CIP non-Gaussian bias is not subtracted off in the standard analysis.

The full *Planck* lensing analysis [29], which includes both CMB temperature and polarization maps, computes a minimum-variance (mv) estimator from all possible CMB map auto and cross correlations, as discussed in detail in Appendixes A and B. The *Planck* lensing estimator relies on maps constructed from the 143 GHz and 217 GHz channels. We furthermore note that the *Planck* analysis uses a bandpass filter in harmonic space to restrict the power spectrum multipoles to $100 \le l \le 2048$.

The full CIP contribution to the lensing-potential estimator for the *Planck* satellite (computed using the full-sky expressions discussed in Appendix B) is shown in the solid red curve in Fig. 2 for $\Delta^2_{\mathrm{rms}}(R_{\mathrm{CMB}}) = 4.3\times10^{-3}$. We can see that both the Gaussian and non-Gaussian CIP contributions to the lensing estimator (dotted red and dotted-dashed purple curves) are negligible compared to the lensing-potential power spectrum (solid yellow); the only significant CIP contribution is given by $L^2C_L^{\Delta\Delta}[Q^{TT}(L)]^2$. The dashed green curve shows the Gaussian noise in a minimum-variance estimator using *Planck*.

Next we develop an approximate expression for the CIP contribution in order to explore its dependence on $L$ and the cosmological parameters. We remind the reader that none of our detailed results/constraints are subject to these approximations, which are developed merely to build intuition for scalings and degeneracies. Since $h_{TT}$ is composed of a sum of $C_l^{T,dT}$, we know that it is only significant on scales smaller than the horizon at decoupling, i.e., $l \gtrsim l_{\mathrm{hor}} \simeq 100$. Therefore, for values of $L \ll l_{\mathrm{hor}}$ the integrand in the numerator of Eq. (51) is dominated by $l_1 \gg L$. In this limit $h_{TT}(\vec{l}_1,\vec{l}_2 \equiv \vec{L}-\vec{l}_1)$ is nearly independent of $L$ and, using the roughly sinusoidal solutions for wave amplitudes in the baryon-photon plasma, can be approximately written as

$$h_{TT}(\vec{l}_1,\vec{l}_2) \simeq 2C_{l_1}^{T,dT} \simeq 2\frac{A_s}{\pi l_1^2}\frac{\partial \ln c_s}{\partial\Delta}[1-\cos(l_1/l_{\mathrm{hor}})], \quad (54)$$

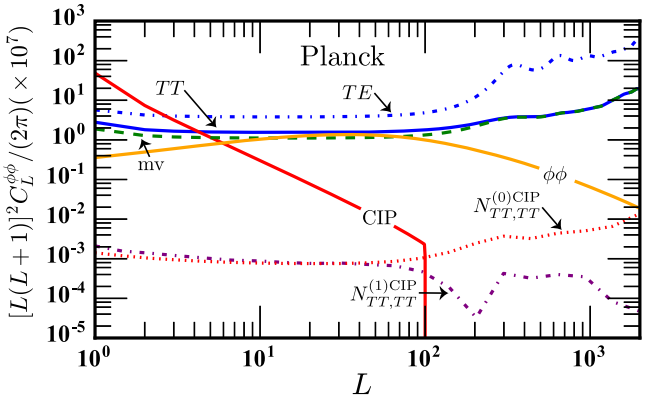


FIG. 2. The CIP contribution to the expectation value of the lensing-potential power-spectrum estimator for *Planck* with $\Delta^2_{\mathrm{rms}} = 4.3\times10^{-3}$. The solid orange curve shows the lensing-potential power spectrum. The blue curves show the Gaussian noise from the $TT$ estimator (solid) and the $TE$ estimator (dotted-dashed). The dashed green curve shows the noise of the minimum-variance estimator. The dashed red curve shows the residual CIP contribution to the Gaussian noise if it is not subtracted from the signal and the purple dot-dashed curve shows the non-Gaussian (i.e., connected part of the trispectrum) CIP contribution. The solid red curve shows the dominant CIP contribution to the estimator.

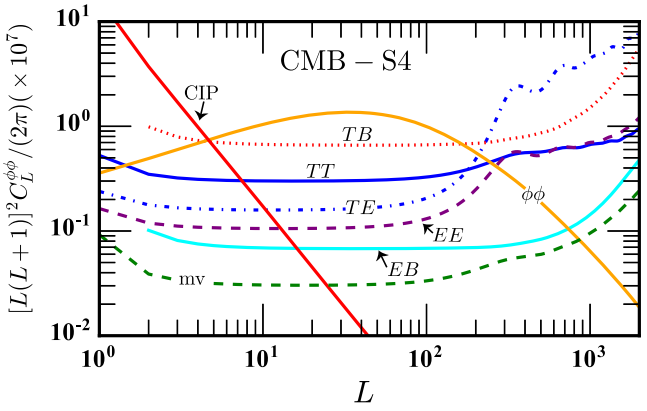


FIG. 3. The CIP contribution to the expectation value of the lensing-potential power-spectrum estimator for a cosmic variance-limited estimate of $C_L^{\phi\phi}$ with $\Delta^2_{\rm rms}(R_{\rm CMB}) = 4.3 \times 10^{-3}$. The expected $C_L^{\phi\phi}$ is shown in solid orange. The Gaussian noise associated with the $TT$, $TE$, $TB$, $EB$, and $EE$ estimators is shown in the solid blue, dotted-dashed blue, dotted red, solid cyan, and dashed purple lines, respectively. The minimum-variance estimator is the dotted green curve, and the solid red curve shows the CIP contribution.

where

$$\frac{\partial \ln c_s}{\partial \Delta} = -\frac{3\Omega_b}{6\Omega_b + 8(1+z_{\rm dec})\Omega_\gamma} \tag{55}$$

is the derivative of the photon-baryon sound speed at decoupling, and $A_s$ is the amplitude of the primordial scalar perturbations. In the same limit we have

$$\begin{aligned} f_{TT}(\vec{l}_1, \vec{l}_2) &= \vec{L}\cdot\vec{l}_1 (C^{TT}_{l_1} - C^{TT}_{|\vec{l}_1 - \vec{L}|}) + L^2 C^{TT}_{|\vec{l}_1 - \vec{L}|}, \\ &\simeq L^2 C^{TT}_{l_1}, \end{aligned} \tag{56}$$

which gives,

$$F_{TT}(\vec{l}_1, \vec{l}_2) \simeq \frac{L^2}{2C^{TT}_{l_1}}, \tag{57}$$

where we used the fact that since $l_1 \gg L$ we have $C^{TT}_{|\vec{l}_1 - \vec{L}|} \simeq C^{TT}_{l_1}$. Combining these expressions, we then find that for $L \ll l_{\rm hor}$ the numerator of Eq. (51) can be approximated by

$$\int \frac{d^2 l_1}{(2\pi)^2} h_{TT}(\vec{l}_1, \vec{l}_2) F_{TT}(\vec{l}_1, \vec{l}_2) \simeq \frac{\partial \ln c_s}{\partial \Delta} L^2 \frac{l^2_{\rm max}}{4\pi}. \tag{58}$$

We will now compute the integrand in the denominator of Eq. (51) using an approximate form for the CMB power spectrum, $C_l^{TT} = A_s/(\pi l^2)$. From this simplified power spectrum we are able to compute the denominator of Eq. (51) and find

$$\int \frac{d^2 l_1}{(2\pi)^2} f_{TT}(\vec{l}_1, \vec{l}_2) F_{TT}(\vec{l}_1, \vec{l}_2) \simeq L^4 \frac{l^2_{\rm max}}{16\pi}. \tag{59}$$

Note that the $L^4$ scaling in Eq. (59) is apparent in the fact that the Gaussian noise curves [given by Eq. (49)] in Figs. 2 and 3 are relatively flat. Combining these expressions we have that

$$Q^{TT}(L) \simeq \frac{4}{L^2}\frac{\partial \ln c_s}{\partial \Delta}. \tag{60}$$

Finally, the CIP contribution to the expectation value of the lensing estimator normalized as in Figs. 2 and 3 is given by

$$L^4 \langle \hat{C}_L^{\phi\phi} \rangle \simeq L^4 C_L^{\phi\phi} + \frac{16 A_{\rm CIP}}{L^2}\left(\frac{\partial \ln c_s}{\partial \Delta}\right)^2. \tag{61}$$

This shows that the CIP contribution to the normalized lensing-potential power-spectrum estimator scales as $1/L^2$, which agrees with the CIP contribution shown in Fig. 5 as well as the values given in Table II.

The approximate expression for the CIP contribution to the lensing-potential power-spectrum estimator in Eq. (60) allows us to estimate the extent to which this contribution varies with cosmological parameters. Given that $d\ln c_s/d\Delta$ in Eq. (55) depends only on the baryon density, we can see that variation of $\Omega_b$ causes the largest variation in the CIP contribution. In particular, we expect a variation of $Q^{TT}(L)$ of order

$$\frac{\delta Q^{TT}(L)}{Q^{TT}(L)} \simeq \left(\frac{1}{\Omega_b} - \frac{1}{\Omega_b + 4(1+z_{\rm dec})\Omega_\gamma/3}\right)\delta\Omega_b. \tag{62}$$

When using the lensing-potential power-spectrum estimates to constrain the CIP amplitude, we find that $\Omega_b = 0.0486 \pm 0.0014$ at 95% CL uncertainty and $\Omega_\gamma \simeq 10^{-4}$ and $z_{\rm dec} \simeq 1100$. With this we find that the variation in $Q^{TT}(L)$ due to the allowed range of $\Omega_b$ is about 2%; as a result, we evaluate $Q^{TT}(L)$ on the fiducial cosmology stated in the Introduction. Also note that the CIP contribution is nearly independent of the noise properties of the experiment.

We show the $Q_L^{XX'}$ computed with the exact expression detailed in Appendix B in Fig. 4. The optimal temperature and polarization estimator is a weighted sum of each correlated map, as described in more detail in Appendixes A and B [28,40,41]. The weights are roughly given by the inverse of the Gaussian noise intrinsic to each map. For example, the Gaussian noise shown in Fig. 2 implies that for the *Planck* satellite the $TT$ CMB map dominates the optimal estimator.

For a futuristic experiment we consider the CMB-S4 experiment, which has the noise properties described in Table I leading to a significantly improved measurement of the polarization of the CMB. CMB-S4 is expected to be

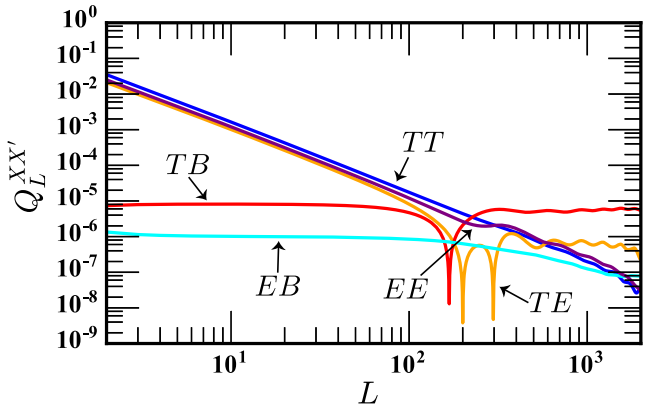


FIG. 4. The CIP contribution to the estimator for the lensing-potential power spectrum, $Q_L^{XX'}$. To produce these curves we used the multipole ranges applicable to CMB-S4 [35].

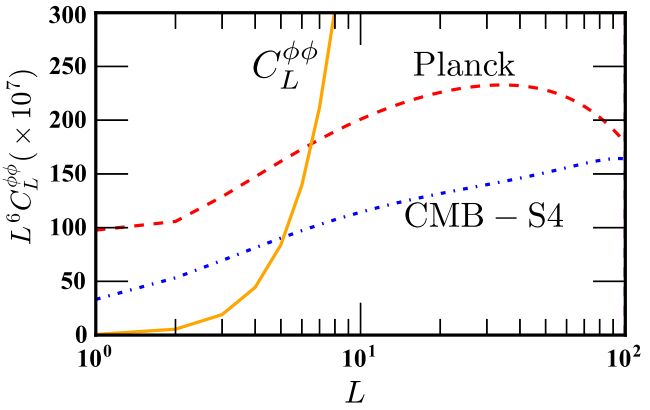


FIG. 5. The CIP contribution to the estimator for the lensing-potential power spectrum for both *Planck* (dashed red) and CMB-S4 (dotted-dashed blue) for $\Delta^2_{\rm rms}(R_{\rm CMB}) = 4.3 \times 10^{-3}$. For comparison, the lensing-potential power spectrum is shown in the solid orange curve.

sensitive to the primordial polarization anisotropies up to $l_{P,\rm max} \simeq 5000$ and to temperature $l_{T,\rm max} \simeq 3000$; since it is a ground-based telescope, it will probe multipoles down to $l_{\rm min} \simeq 30$ [35]. As shown in Fig. 3, in this case the *EB* cross-correlated CMB map dominates the optimal lensing-potential estimator. Figure 4 shows, however, that the CIP contributions of $Q_L^{EB}$ are much smaller than any other combination. As a result, the CIP contribution to CMB-S4 is *less* than that for *Planck* (see Fig. 5). Of course, CMB-S4 is significantly more sensitive to CIPs than *Planck* when using the optimal CIP estimator, as we explain in Sec. VI.

We can understand the qualitative behaviors of the $Q_L^{XX'}$ shown in Fig. 4 by noting that, in the absence of any primordial B-mode polarization, the CIP modulation induces contributions to the temperature and polarization of the form (see Appendix A for a derivation)

$$\delta T_\Delta(\vec{l}) = \int \frac{d^2 l_1}{(2\pi)^2} \frac{\partial T(\vec{l}_1)}{\partial \Delta} \Delta(\vec{L}), \tag{63}$$

$$\delta E_\Delta(\vec{l}) = \int \frac{d^2 l_1}{(2\pi)^2} \frac{\partial E(\vec{l}_1)}{\partial \Delta} \Delta(\vec{L}) \cos 2\varphi_{\vec{l}_1 \vec{l}}, \tag{64}$$

TABLE I. *Planck* sensitivity in the 143 and 217 GHz channels to temperature and polarization at the two frequencies used to estimate the lensing potential [29,42]. The last line gives the sensitivity for CMB-S4, a proposed next generation CMB telescope [35].

| Channel | $\theta$ (arcmin) | $w_T(\mu$K arcmin) | $w_P(\mu$K arcmin) |
|---|---|---|---|
| 143 GHz | 7 | 30 | 60 |
| 217 GHz | 5 | 40 | 95 |
| CMB-S4 | 3 | 1 | 1.4 |

$$\delta B_\Delta(\vec{l}) = \int \frac{d^2 l_1}{(2\pi)^2} \frac{\partial E(\vec{l}_1)}{\partial \Delta} \Delta(\vec{L}) \sin 2\varphi_{\vec{l}_1 \vec{l}}, \tag{65}$$

where $\vec{L} \equiv \vec{l} - \vec{l}_1$ and $\varphi_{\vec{l}_1 \vec{l}}$ is the angle between the flat-sky wave vectors $\vec{l}_1$ and $\vec{l}$. Since $\Delta(\vec{L})$ is drawn from a scale-invariant power spectrum, its largest contribution will come from the smallest values of $L$. This implies that for large values of $l$, since the three vectors $\vec{l}$, $\vec{l}_1$, and $\vec{L}$ form a triangle, we must have $\vec{l}_1$ and $\vec{l}$ nearly parallel. In particular, it is straightforward to show that in this limit $\sin 2\varphi_{\vec{l}_1 \vec{l}} \simeq 2(L/l)\sin\phi$, where $\phi$ is the angle that $\vec{l}_1$ makes with the $x$ axis. Similarly, in this limit we have $\cos 2\varphi_{\vec{l}_1 \vec{l}} \simeq 1$. The lensing contributions to the CMB anisotropies have the same dependence on $\varphi_{\vec{l}_1, \vec{l}}$. Therefore, given that $Q^{XX'} \sim h_{XX'} f_{XX'}$ (these functions are given in Table V in Appendix A), we expect the following scalings for the CIP contributions to the standard lensing estimator with $L$: $Q^{XE}(L) \propto Q^{TT}(L)$ and $Q^{XB}(L)/Q^{XE}(L) \propto L^2$. In addition, because $|\sin 2\varphi_{\vec{l}_1 \vec{l}}| \ll 1$, we expect that for small values of $L$, $Q^{XB}(L)$ will be much smaller than any other CIP contribution. Finally, in Fig. 4 we can see that $Q_L^{TE}$ changes slope at roughly the acoustic horizon, $L \simeq 100$. This change occurs because the two terms that make up this contribution, $C_l^{T,dE} + C_{|\vec{l}-\vec{L}|}^{E,dT}$, are of opposite sign and out of phase by half of a period $\Delta l \simeq 100$ (see Fig. 8 of Ref. [22]). Therefore, while $L < 100$ the CIP response remains constant, leading to a decrease in $Q_L^{TE} \propto L^{-2}$, but for $L \gtrsim 100$ the CIP response *grows*, leading to $Q_L^{TE} \simeq$ constant (also see Sec. III. D of Ref. [18]).

We show the first ten values of the exact CIP contribution to both *Planck* and CMB-S4 in Table II. We stress that

TABLE II. CIP contribution, with $\Delta^2_{\rm rms}(R_{\rm CMB}) = 1$, to the normalized lensing-potential estimator, $[L(L+1)]^2\hat{C}^{\phi\phi}_L/(2\pi)$, for *Planck* and CMB-S4 given by Eq. (B12).

| $L$ | *Planck* | CMB-S4 |
|---|---|---|
| 1 | $4.51 \times 10^{-3}$ | $1.54 \times 10^{-3}$ |
| 2 | $6.87 \times 10^{-4}$ | $3.46 \times 10^{-4}$ |
| 3 | $2.94 \times 10^{-4}$ | $1.58 \times 10^{-4}$ |
| 4 | $1.66 \times 10^{-4}$ | $9.17 \times 10^{-5}$ |
| 5 | $1.07 \times 10^{-4}$ | $6.00 \times 10^{-5}$ |
| 6 | $7.55 \times 10^{-5}$ | $4.24 \times 10^{-5}$ |
| 7 | $5.61 \times 10^{-5}$ | $3.16 \times 10^{-5}$ |
| 8 | $4.33 \times 10^{-5}$ | $2.45 \times 10^{-5}$ |
| 9 | $3.44 \times 10^{-5}$ | $1.96 \times 10^{-5}$ |
| 10 | $2.81 \times 10^{-5}$ | $1.60 \times 10^{-5}$ |
| >10 | $(L/0.053)^{-2}$ | $(L/0.032)^{-1.92}$ |

when computing the values and scalings given in Table II we have made no approximations, as opposed to the rough estimate given in Eq. (60). In order to compute the specific CIP contribution, the values in Table II need to be multiplied by $\Delta^2_{\rm rms}(R_{\rm CMB})$. For $11 \leq L \leq 40$ both the *Planck* and CMB-S4 CIP contributions to $[L(L+1)]^2\hat{C}^{\phi\phi}_L/(2\pi)$ are well-fit (to within a few percent) by a power law of the form $(L/L_0)^{-\alpha}$ with $(L_0,\alpha) = (0.053, 2.0)$ for *Planck* and $(L_0,\alpha) = (0.032, 1.92)$ for CMB-S4.

Figure 6 gives a sense of the sensitivity of the *Planck* lensing measurements to CIPs. We can see that it is the lowest-$L$ data that provides the constraint on $\Delta^2_{\rm rms}(R_{\rm CMB})$. Although in principle the *Planck* measurements can be extended to even lower $L$ values, in practice estimates of the lensing-potential power spectrum are not robust for $L < 8$ [29].

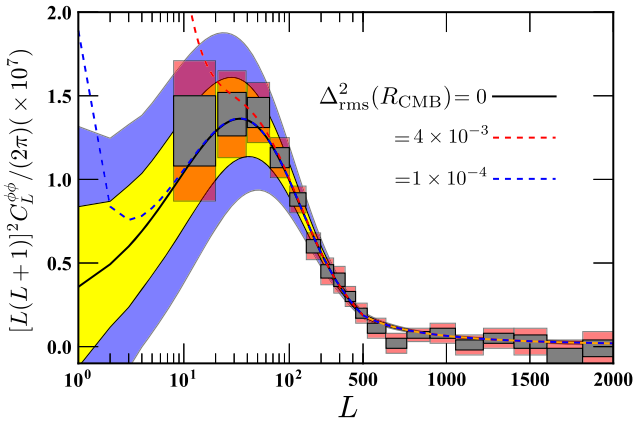


FIG. 6. *Planck* estimates of the lensing-potential power spectrum from Ref. [29] along with the expectation value of the lensing-potential power spectrum for three values of $\Delta^2_{\rm rms}(R_{\rm CMB})$. We also show the 68% (yellow region) and 95% (blue region) CL for a cosmic variance–limited estimate of $C^{\phi\phi}_L$.

## IV. PREVIOUS CONSTRAINTS TO COMPENSATED ISOCURVATURE PERTURBATIONS

On scales probed by current cosmological observations (i.e., $k \lesssim 10$ Mpc$^{-1}$) CIPs lead to a spatial fluctuation of the baryon density beyond the adiabatic prediction. These fluctuations can affect several different observables, such as the primordial light-element abundances and the baryon fraction in galaxies and galaxy clusters [23]. It can also lead to anomalous angular correlations in observations of the baryon acoustic oscillations (BAOs).

Any probe of the spatial dependence of the cosmological baryon fraction has the potential to be sensitive to CIPs. Past work has concentrated on placing constraints on the CIP amplitude through off-diagonal contributions to the CMB four-point correlation function [34], smoothing of the small-scale CMB power spectra [26,27], fluctuations in the baryon fraction of galaxy clusters [23], spatial variation in the primordial deuterium to hydrogen (D/H) ratio measured in quasar absorption lines [23], and an additional offset between the large-scale distribution of total mass from luminous (i.e., baryonic) matter [24]. These constraints probe the CIP modulation on a variety of length scales. We will use Eq. (17) to convert a constraint on the CIP variance $\Delta^2_{\rm rms}(R)$ to a constraint on the scale-invariant CIP amplitude, $A_{\rm CIP}$. Since the integral over $k$ formally diverges at large scales (i.e., small values of $k$) we take $k_{\rm min}$ to be of the order of the current horizon, $k_{\rm min} \simeq (10\ {\rm Gpc})^{-1}$.

### A. Nucleosynthesis bounds

The primordial abundance of the light elements is, in part, determined by the local baryon-to-photon ratio, $\eta \equiv n_b/n_\gamma$. Under the assumption of adiabatic initial conditions, $\eta$ is spatially uniform; in the presence of a CIP it will be modulated by the CIP field, $\Delta$. Measurements of the primordial helium abundance ($Y_p$) and the D/H ratio in several galaxies allow us to place constraints on any intrinsic scatter in their values. The measurements of $Y_p$ and D/H place upper limits on $\Delta_{\rm rms}(R_{\rm gal})$, the rms variation of $\Delta$ on galactic scales. In the presence of a CIP the Helium abundance, $Y_p$, varies as $\Delta Y_p \simeq 0.0087\Delta_{\rm rms}(R_{\rm gal})$, and D/H as $\Delta \log[{\rm D/H}] \simeq 0.69\Delta_{\rm rms}(R_{\rm gal})$ [23]. We will take $R_{\rm gal} \sim 1$ Mpc to be the typical size of the region that collapses to form the galaxies in which $Y_p$ and D/H are measured and find that $\Delta^2_{\rm rms}(R_{\rm gal}) = 3.57A_{\rm CIP}$. Upper limits to the variation in $Y_p$ and D/H give (at 95% CL) $\Delta_{\rm rms}(R_{\rm gal}) < 0.25$ leading to $A_{\rm CIP} < 0.13$.

### B. Baryon-gas fraction bounds

In the presence of a CIP the ratio $\delta_b/\delta_c$ becomes scale dependent. The gas fraction of a galaxy cluster directly probes any fluctuation between baryons and dark matter.

TABLE III. Best-fit values and standard deviations for cosmological parameters with the three different *Planck* data sets as described in the text. All upper limits to $\Delta^2_{\rm rms}$ show 95% CL. The 68% CL uncertainty in $\Delta^2_{\rm rms}$ is $\pm 0.0055$ when using T + LowP.

| Parameter | T + LowP | T + P | T + P + lensing |
|---|---|---|---|
| $\omega_b$..... | $0.02277 \pm 0.00034$ | $0.02245 \pm 0.00020$ | $0.02234 \pm 0.0016$ |
| $\omega_c$..... | $0.1166 \pm 0.0025$ | $0.1189 \pm 0.0016$ | $0.1186 \pm 0.0014$ |
| $n_s$..... | $0.979 \pm 0.0085$ | $0.969 \pm 0.0056$ | $0.967 \pm 0.0048$ |
| $\log(10^{10}A_s)$ | $3.061 \pm 0.040$ | $3.069 \pm 0.036$ | $3.04 \pm 0.025$ |
| $\tau$..... | $0.067 \pm 0.02$ | $0.068 \pm 0.018$ | $0.054 \pm 0.014$ |
| $H_0$..... | $69.2 \pm 1.3$ | $67.8 \pm 0.75$ | $67.83 \pm 0.65$ |
| $\Delta^2_{\rm rms}$..... | $0.014 \pm 0.011$ | $<0.0139$ | $<0.00434$ |

Reference [23] found that $\Delta_{\rm rms}(R_{\rm cl}) < 0.08$ at 95% CL. With $R_{\rm cl} \simeq 10$ Mpc we have $\Delta^2_{\rm rms}(R_{\rm cl}) = 0.49 A_{\rm CIP}$ and $A_{\rm CIP} < 0.017$ at 95% CL. It is also possible to look for statistical fluctuations in the baryon and dark matter fluctuations. Using measurements of the baryon acoustic oscillations on scales $R \sim 100$ Mpc, Ref. [24] found an upper limit of $A_{\rm CIP} < 0.064$, which translates into $\Delta^2_{\rm rms}(R = 100\ {\rm Mpc}) < 0.0165$.

### C. Past CMB bounds

As we saw in Sec. III, the CIP modulation smooths the CMB power spectra and contributes to the CMB trispectrum. Constraints from the first effect (under a Gaussian-likelihood approximation [26]) yield the constraint $A_{\rm CIP} < 0.04$ at 95% CL when using both temperature and polarization. In Ref. [34] the CIP contribution to the full trispectrum was constrained using WMAP data, yielding $A_{\rm CIP} < 0.044$ at 95% CL. Recently, using temperature and polarization power-spectra results from *Planck*, Ref. [27] found the constraint $\Delta^2_{\rm rms}(R_{\rm CMB}) < 0.012$ $(A_{\rm CIP} < 0.050)$ at 95% CL. When using the *Planck* estimates of the lensing power spectrum, Ref. [27] uses the conservative lensing likelihood in the range $40 \le L \le 400$ and neglects to include the CIP contribution to the estimator of the lensing-potential power spectrum. We use the aggressive *Planck* lensing dataset in the range $8 \le L \le 2048$, which breaks the degeneracies slightly better than the conservative lensing dataset and provides direct extra constraining power on CIP at low $L$ due to the effect we have studied in this paper. Our full analysis thus improves upon the constraint in Ref. [27] by a factor of ∼3.

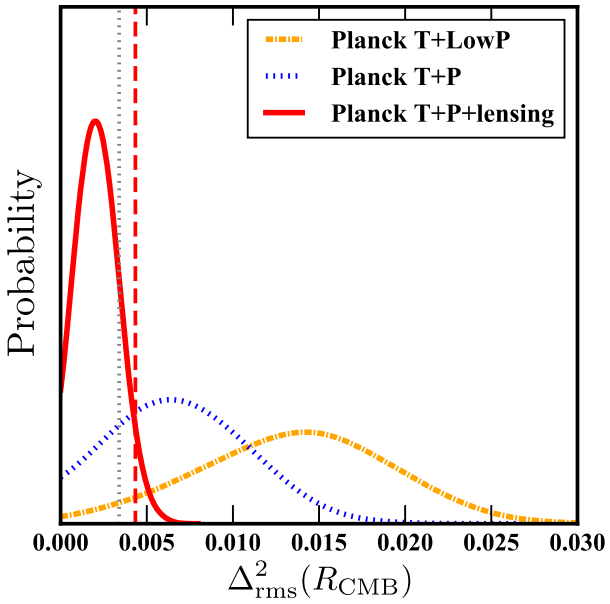


FIG. 7. The 1D marginalized posterior for $\Delta^2_{\rm rms}(R_{\rm CMB})$ using the three combinations of data sets discussed in the text. The vertical dashed line indicates the 95% CL upper limit using the T + P + lensing data sets. The vertical dotted line shows the expected 95% CL upper limit if we were to apply the optimal CIP estimator to the *Planck* measurements of the CMB. The proximity of these two limits shows that, when considering a constraint to the overall amplitude of the CIP modulation, the analysis presented here is nearly optimal.

## V. CONSTRAINTS TO CIPS FROM *PLANCK* MEASUREMENTS OF THE CMB

To explore *Planck*'s sensitivity to CIPs we modified the publicly available Boltzmann solver CAMB[1] to compute the CIP-modulated CMB power spectra (as described in Appendix D) and CIP-modified expectation value of the lensing-potential estimator given by Eq. (B12). In particular, we modified CAMB to compute the sum of the lensing-potential power spectrum and the CIP contribution, given in Table. II. We compared these theoretical predictions to the *Planck* data using the publicly available *Planck*-likelihood code [7] and the Markov Chain Monte Carlo (MCMC) code COSMOMC[2] [43].

The *Planck* data has been divided up into a large angular-scale data set (low multipole number) and a small angular-scale data set (high multipole number) [7]. For all constraints we use the entire range of measurements for the $TT$ power spectrum as well as the low multipole polarization ($TE$ and $EE$) data, which we denote as "T + LowP." We also compute constraints using the entire multipole range of

[1] http://camb.info
[2] http://cosmologist.info/cosmomc/

polarization measurements, denoted by "T + P." The division between these two data sets is the multipole number $l = 29$ which approximately corresponds to an angular scale of $\simeq 5°$. In addition to the temperature and polarization power spectra, we use the *Planck* estimate of the lensing-potential power spectrum [29]. Since the CIP contribution to the standard lensing estimator is largest on the largest angular scales, we use the "aggressive" estimate of the lensing-potential power spectrum which extends down to $L_{\rm min} = 8$. We used the PLIK likelihood [7] and varied all 27 *Planck* nuisance parameters.

As demonstrated in Fig. 1, polarization data can break degeneracies present in a temperature-only analysis. The top panel in Fig. 1 shows that the residual $TT$ power spectrum has an oscillating structure around $l \simeq 1000$. When comparing the CIP modulation of the $TT$ power spectrum, we can see by eye that a nonzero CIP amplitude can fit these residuals. As shown in the first column of Table III, this is reflected by the fact that the T + LowP data sets prefer a nonzero CIP modulation with $\Delta^2_{\rm rms}(R_{\rm CMB}) = 0.014 \pm 0.011$ at 95% CL (corresponding to $A_{\rm CIP} = 0.056 \pm 0.044$). When we include the full polarization measurements from *Planck* (i.e., T + P),

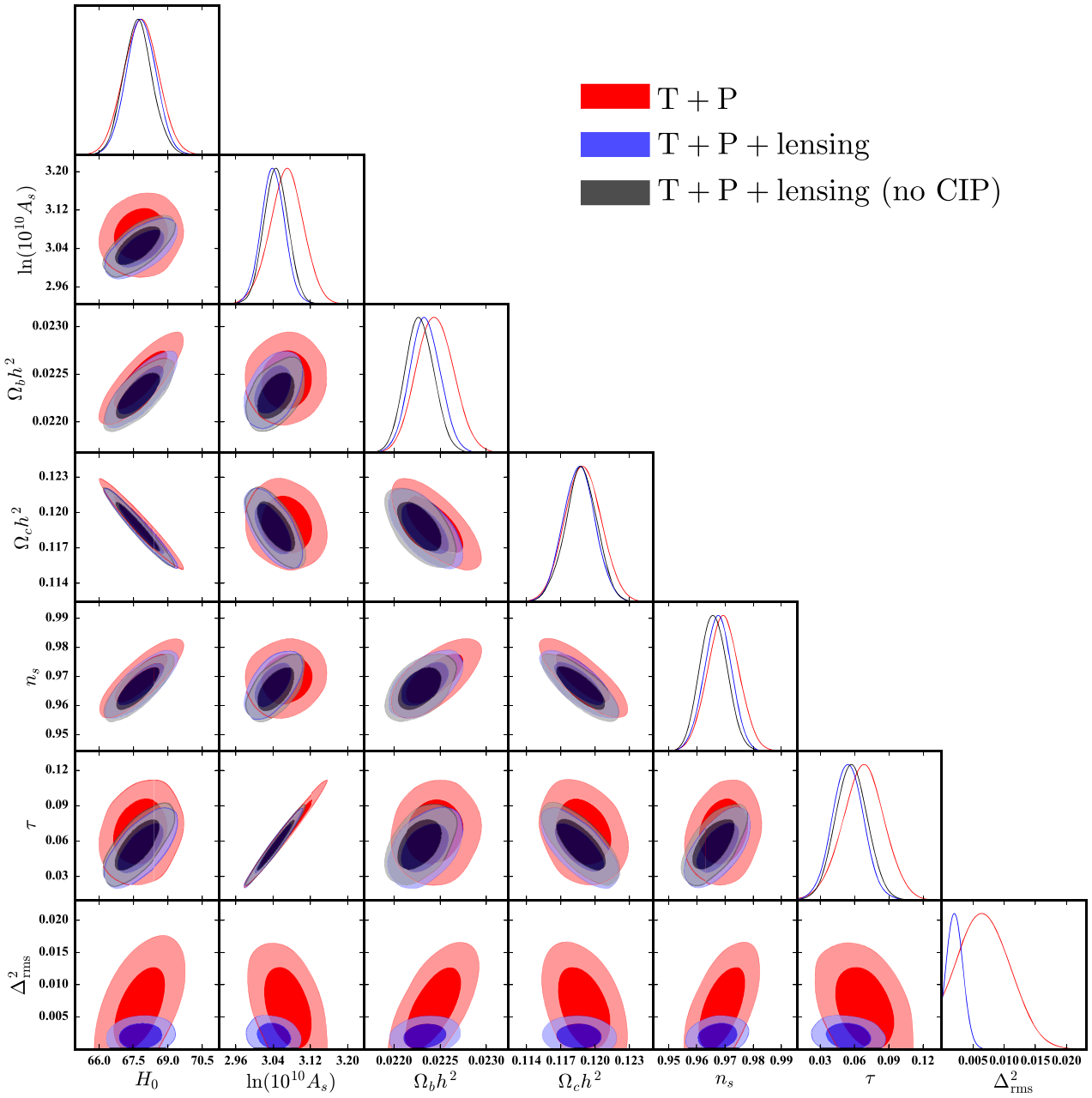


FIG. 8. A "triangle plot" showing the 2D marginalized posteriors for the standard six cosmological parameters and the CIP rms variation on cosmological scales, $\Delta^2_{\rm rms}(R_{\rm CMB})$.

the upper limit to the CIP mode decreases to $< 0.0139$ at 95% CL ($A_{\rm CIP} < 0.056$). Figure 1 indicates this is mainly due to precise measurements of $C_l^{EE}$ at multipoles between $30 \lesssim l \lesssim 400$. Finally, when including estimates of the lensing-potential power spectrum (i.e., T + P + lensing), the upper limit to the CIP modulation decreases by a factor of ∼3.2.

The 1D marginalized posterior on $\Delta^2_{\rm rms}(R_{\rm CMB})$ using the three combinations of data sets is shown in Fig. 7. We can see how the CIP contribution to the lensing-potential power spectrum significantly improves the sensitivity to $\Delta^2_{\rm rms}(R_{\rm CMB})$. This figure also makes clear how the position of the maximum of the 1D posterior decreases as we add in additional data.

In order to explore any degeneracies in these parameters, we show a "triangle plot" for the standard six cosmological parameters and $\Delta^2_{\rm rms}(R_{\rm CMB})$ in Fig. 8. As shown by a comparison between the black and blue contours, the constraints on the standard six parameters remain fairly unchanged when we additionally constrain $\Delta^2_{\rm rms}(R_{\rm CMB})$. Moreover, going from T + P to T + P + lensing clearly reduces the overall uncertainties of $\Delta^2_{\rm rms}(R_{\rm CMB})$, as well as its correlations with the rest of ΛCDM parameters, since the information on the CIPs comes from the large-scale lensing estimator.

## VI. CIP SENSITIVITY OF FUTURE EXPERIMENTS

We now assess the sensitivity of future CMB experiments to CIPs. As for lensing, the improvements will come primarily from small scales (in particular, polarization), and so we focus on the proposed CMB-S4 experiment, as described in Ref. [44]; CMB-S4 will be a nearly cosmic variance–limited (CVL) experiment in both temperature and polarization. Our analysis can be easily implemented using noise specifications for other future experiments.

We model CMB-S4 as a single-channel experiment, as described in Table I, observing in the range $30 \le l \le 3000$ for temperature and $30 \le l \le 5000$ for polarization (due to the smaller relative amplitude of small-scale polarized foregrounds). Given these characteristics, the lensing noise can be computed as in Refs. [28,45]. We show the CVL case in Fig. 6.

### A. Lensing-potential bias and power-spectrum smoothing

The sensitivity of lensing-potential bias and power-spectrum smoothing to CIPs is estimated using the Fisher matrix [46–50]

$$F_{ij} = \sum_l \frac{2l+1}{2} f_{\rm sky} {\rm Tr}\left[\mathbf{C}_l^{-1}\frac{\partial \mathbf{C}_l}{\partial p_i}\mathbf{C}_l^{-1}\frac{\partial \mathbf{C}_l}{\partial p_j}\right], \quad (66)$$

where $p_i$ contains the six ΛCDM parameters plus the CIP variance $\Delta^2_{\rm rms}$, and the CMB covariance matrix is given by

$$\mathbf{C}_l = \begin{pmatrix} C_l^{TT,{\rm t}} & C_l^{TE,{\rm t}} & C_l^{Td,{\rm t}} \\ C_l^{TE,{\rm t}} & C_l^{EE,{\rm t}} & 0 \\ C_l^{Td,{\rm t}} & 0 & C_l^{dd,{\rm t}} \end{pmatrix}, \quad (67)$$

where all of the power spectra are computed from the observed maps as in Eqs. (23) and (24), following the noise properties from Table I with zero noise for any cross-correlated (i.e., $TE$) maps. Since the CIP contribution to the lensing-potential power-spectrum estimator roughly decreases as $L^{-2}$, the sensitivity of future estimates to the scale-invariant CIP amplitude, $A_{\rm CIP}$, is highly dependent on the minimum observable $L$ value, $L_{\rm min}$, and therefore highly dependent on the sky coverage. Assuming that the nonlensing biases contributing to the lensing-potential power-spectrum estimator can be robustly subtracted on large angular scales, the minimum multipole which can be estimated is approximately given by $L_{\rm min} \sim f_{\rm sky}^{-1/2}$. Unfortunately, galactic foregrounds [51] and temperature/polarization leakage [44] could degrade the largest-scale measurements ($L < 30$).

We defer analysis of these complications to future work and obtain forecasts as a function of the minimum $L_{\rm min}$ detectable by the CMB-S4. Using information from the lensing estimator and power-spectrum smoothing, we obtain the sensitivity to $\Delta^2_{\rm rms}(R_{\rm CMB})$ for the CMB-S4 experiment as a function of $L_{\rm min}$ (shown in Fig. 9). For $L_{\rm min} \ge 10$ the majority of the constraint comes from the CIP modulation of the CMB power spectrum, whereas for $L_{\rm min} < 10$ the CIP contribution to the lensing-potential estimator dominates. We note that the CMB-S4 lensing noise is very close to the cosmic-variance limit, and therefore the results should be the same for any other

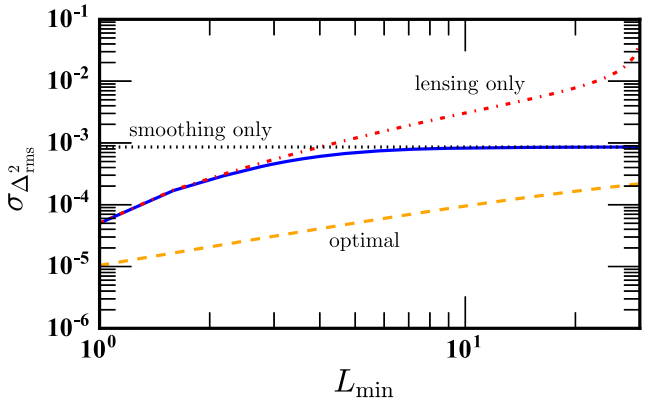


FIG. 9. Projected sensitivity to $\Delta^2_{\rm rms}(R_{\rm CMB})$ for CMB-S4. The overall sensitivity is shown in the solid blue curve. The sensitivity can be divided into a contribution from the smoothing of the CMB multipoles (dotted black) and from estimates of the lensing-potential power spectrum (dotted-dashed red). The optimal estimator is shown in the dashed orange curve. As is clear from this figure, the CIP lensing-potential contribution is only important if future experiments can probe $L_{\rm min} \lesssim 5$.

TABLE IV. Current constraints on $A_{\rm CIP}$, the amplitude of the power spectrum of a scale-invariant CIP modulation field. All uncertainties and upper limits are at 95% CL.

| Method | $A_{\rm CIP}$ |
|---|---|
| Trispectrum, WMAP [34] | $<0.044$ |
| Baryon Acoustic Oscillations [24] | $<0.064$ |
| Baryon Fraction in Galaxy Clusters [23] | $<0.017$ |
| Dispersion in $^4$He and D/H [23] | $<0.13$ |
| CMB T + P + high-$L$ lensing [27] | $< 0.050$ |
| *This work*: | |
| *Planck* T + LowP | $0.056 \pm 0.044$ |
| *Planck* T + P | $<0.056$ |
| *Planck* **T + P + lensing** | $<$**0.017** |

nearly CVL experiment. In particular, a full-sky CVL measurement of the lensing-potential power spectrum has the potential to constrain $\Delta^2_{\rm rms}(R_{\rm CMB}) \lesssim 10^{-5}$, and therefore $A_{\rm CIP} \lesssim 4 \times 10^{-5}$. We now turn our attention to additional improvements possible with an optimal estimator of CIPs.

### B. Optimal estimator

The constraints obtained in this work from the observed CMB trispectrum rely on the contribution of CIPs to the lensing-potential estimator. There is, however, an optimal CIP estimator which relies on the distinct (from lensing) off-diagonal CMB multipole correlations induced by CIPs, as shown in Refs. [18,21,22] and summarized in Appendixes B and E. This estimator was used to obtain the WMAP constraints to CIPs in Ref. [34]. The Fisher information, $F$, which yields the minimum uncertainty $\sigma_{\Delta^2_{\rm rms}} = \sqrt{1/F}$, is given by

$$F = \sum_L \frac{(2L+1)}{2} f_{\rm sky} \left( \frac{\partial C_L^{\Delta\Delta}}{\partial \Delta^2_{\rm rms}} \right)^2 (N_L^{\Delta\Delta})^{-2}, \quad (68)$$

where $N_L^{XX'}$ are defined in Ref. [34] and computed under the null hypothesis. We use Eq. (68) to forecast the sensitivity of *Planck* and CMB-S4 (although *Planck* data are public, we still have to "forecast" its sensitivity given that a full analysis of the *Planck* CMB trispectrum for CIPs does not yet exist) to a scale-invariant angular power spectrum of CIPs.

For *Planck* noise parameters, we find that the optimum estimator has a $2\sigma$ sensitivity of $\Delta^2_{\rm rms}(R_{\rm CMB}) \simeq 4 \times 10^{-3}$, offering no significant improvement over the constraint from the CIP contribution to the lensing-potential estimator (see Fig. 7 for an illustration). In other words, the constraints in Sec. V are nearly optimal using *Planck* data.

On the other hand, for a nearly CVL experiment like CMB-S4, the optimal estimator improves on the constraint from the CIP contribution to the lensing estimator by a factor of $\sim$4.0 for $L_{\rm min} = 1$ and a factor of $\sim$4.5 for $L_{\rm min} = 30$. This difference, illustrated in Fig. 9, is driven by the constraining power of a nearly CVL polarization experiment.

Given the fact that the trispectrum is so much more constraining than the CIP-induced smoothing of the CMB power spectrum, we neglect primary power-spectrum constraints in this Fisher analysis. For futuristic experiments (like CMB-S4), the reconstruction noise for both lensing and CIPs may be low enough that lensing could introduce a significant bias [52] to the estimators described in Appendix E, requiring either a debiased minimum-variance estimator (as discussed in Ref. [53]) or a "delensed" CMB map (as discussed in Refs. [54,55]), in which lensing-induced correlations have been filtered out. We defer an analysis that includes these complications to future work, and simply note that Eq. (68) quantifies the best CIP reconstruction we could achieve using the CMB.

## VII. CONCLUSIONS

We have shown how the presence of a CIP modulation contributes to the lensing-potential power-spectrum estimator. In particular, we have used the *Planck* data to place the most stringent constraints on the amplitude of a scale-invariant CIP modulation, $\Delta^2_{\rm rms}(R_{\rm CMB}) < 4.3 \times 10^{-3}$ at 95% CL, on cosmological scales. The method discussed here provides a nearly optimal upper limit when using *Planck* data. We note that this statement only applies to the overall amplitude of a scale-invariant CIP power spectrum. A full trispectrum analysis could additionally probe the scale dependence of a CIP power spectrum.

We show a comparison of our results to previous constraints to the amplitude scale-invariant CIP power spectrum in Table IV [see Eq. (20) for a translation between $\Delta^2_{\rm rms}(R_{\rm CMB})$ and $A_{\rm CIP}$]. This table shows that before this work the most sensitive constraint to the CIP amplitude came from estimates of the baryon fraction in galaxy clusters. The results presented here are as sensitive to $A_{\rm CIP}$. Furthermore, given that the analysis of the baryon fraction estimates assumes that the clusters are representative of the baryon density throughout the universe and that they are kinematically relaxed [23] the robustness of these constraints may be in question [26]. On the other hand, the CMB-related constraints presented here do not suffer from such complexities and are therefore more straightforward to interpret.

We note that the constraints presented here do not apply to curvaton-generated CIPs, which are correlated with adiabatic fluctuations. In this scenario, the effect of CIPs on CMB observables is enhanced relative to what is considered here. Our limits do, however, give us a conservative upper limit on the sensitivity of our technique to curvaton-generated CIPs.

As discussed in Sec. V, the upper limit to $A_{\rm CIP}$ found here is nearly optimal for the measurements from *Planck*. Looking towards future experiments with nearly ideal sensitivity to polarization, we find that the method

presented here is about a factor of 4.5 less sensitive than the optimal estimator. However, we note that the standard analysis of future CMB data will include an estimate of the lensing-potential power spectrum from the CMB trispectrum. Therefore, the results presented here show that, in the presence of a CIP modulation, we may find excess power in the lensing estimator at large angular scales. This conclusion applies to *any* scale-invariant stochastic field which modulates the CMB. In particular, processes like patchy reionization [56] or a spatial variation in the fine structure constant [57,58] should contribute to the lensing estimator in a similar way. We leave such extensions of the results presented here to future work.

## ACKNOWLEDGMENTS

T. L. S. acknowledges support from the Provost's office at Swarthmore College. J. B. M. is supported by the Simons foundation and NASA ATP Grant No. NNX15AB18G. R. S. acknowledges the support of the Panaphil Foundation though a Velay Scholarship. The authors thank Jussi Valiviita and Chen He Heinrich for useful suggestions and a careful reading of the manuscript. The authors wish to thank Yacine Ali-Haïmoud, Marc Kamionkowski, Michael Kesden, and Marius Millea for interesting and enlightening discussions. R. S. and K. Y. contributed equally to this work.

## APPENDIX A: CIP MODULATION OF THE CMB IN THE FLAT-SKY LIMIT

In the presence of a CIP field the CMB is modulated in a way that is analogous to the effects of gravitational lensing. In this appendix we present the flat-sky expressions for the modulated temperature and polarization. Since we are interested in the leading-order effects on the trispectrum, we only consider terms to linear order in the lensing-potential, $\phi$, and CIP modulation field, $\Delta$.

In the flat-sky approximation we have [28,40,41]

$$(Q \pm iU)(\hat{n}) = -\int \frac{d^2l}{(2\pi)^2}[E(\vec{l}) \pm iB(\vec{l})]e^{\pm 2i\varphi_{\vec{l}}}e^{i\vec{l}\cdot\hat{n}}, \quad \text{(A1)}$$

where $\varphi_{\vec{l}}$ is the polar angle of the wave vector $\vec{l}$. Expanding $[Q \pm iU](\hat{n})$ to linear order in the lensing-potential and the CIP modulation field, we have

$$[Q \pm iU](\hat{n} + \vec{\nabla}\phi, \Delta) \simeq [Q \pm U](\hat{n}) + \nabla_i\phi\nabla^i[Q \pm U] + \Delta(\hat{n})\frac{\partial[Q \pm U]}{\partial\Delta}\bigg|_{\Delta=0}. \quad \text{(A2)}$$

Using the fact that $[Q \pm iU](\vec{l}) = [E(\vec{l}) \pm iB(\vec{l})]e^{\pm 2i\varphi_{\vec{l}}}$ and writing $X_{\rm obs}(\vec{l}) = X(\vec{l}) + \delta X(\vec{l})$, we have

$$\delta T(\vec{l}) = \int \frac{d^2l_1}{(2\pi)^2} W_T(\vec{l}, \vec{l}_1), \quad \text{(A3)}$$

$$\delta E(\vec{l}) = \int \frac{d^2l_1}{(2\pi)^2}[W_E(\vec{l}, \vec{l}_1)\cos 2\varphi_{\vec{l}_1\vec{l}} - W_B(\vec{l}, \vec{l}_1)\sin 2\varphi_{\vec{l}_1\vec{l}}], \quad \text{(A4)}$$

$$\delta B(\vec{l}) = \int \frac{d^2l_1}{(2\pi)^2}[W_B(\vec{l}, \vec{l}_1)\cos 2\varphi_{\vec{l}_1\vec{l}} + W_E(\vec{l}, \vec{l}_1)\sin 2\varphi_{\vec{l}_1\vec{l}}], \quad \text{(A5)}$$

where $\varphi_{\vec{l}_1,\vec{l}} \equiv \varphi_{\vec{l}_1} - \varphi_{\vec{l}}$ and

$$W_X(\vec{l}, \vec{l}_1) \equiv X(\vec{l}_1)W_\phi(\vec{l}_1, \vec{l}) + \frac{\partial X(\vec{l}_1)}{\partial\Delta}\Delta(\vec{l} - \vec{l}_1)$$
$$W_\phi(\vec{l}, \vec{l}_1) \equiv -\phi(\vec{l} - \vec{l}_1)[(\vec{l} - \vec{l}_1)\cdot\vec{l}_1] \quad \text{(A6)}$$

This allows us to write down an estimator for the lensing potential in terms of the various correlations [28,40,41] as follows:

$$\hat{d}_\alpha(\vec{L}) \equiv \frac{A_{XX'}(L)}{L}\int \frac{d^2l_1}{(2\pi)^2}X^t(\vec{l}_1)X'^t(\vec{l}_2)F_{XX'}(\vec{l}_1, \vec{l}_2), \quad \text{(A7)}$$

where $\vec{l}_2 \equiv \vec{L} - \vec{l}_1$, $\alpha = XX'$ and

$$F_{XX'}(\vec{l}_1, \vec{l}_2) \equiv \frac{C_{l_1}^{X'X',\rm t}C_{l_2}^{XX,\rm t}f_{XX'}(\vec{l}_1, \vec{l}_2) - C_{l_1}^{XX',\rm t}C_{l_2}^{XX',\rm t}f_{XX'}(\vec{l}_2, \vec{l}_1)}{C_{l_1}^{XX,\rm t}C_{l_2}^{X'X',\rm t}C_{l_1}^{X'X',\rm t}C_{l_2}^{XX,\rm t} - (C_{l_1}^{XX',\rm t}C_{l_2}^{XX',\rm t})^2}, \quad \text{(A8)}$$

$$A_{XX'}(L) \equiv L^2\left\{\int \frac{d^2l_1}{(2\pi)^2}f_{XX'}(\vec{l}_1, \vec{l}_2)F_{XX'}(\vec{l}_1, \vec{l}_2)\right\}^{-1}. \quad \text{(A9)}$$

We have defined the total CMB power spectrum, $C_l^{XX',\rm t}$, which includes detector noise and finite resolution, in Eq. (23), and we show the $f_{XX'}$ in Table V. The (Gaussian) noise in each estimator is given by

$$N^{(0)}_{\alpha,\beta}(L) = \frac{A_\alpha(L)A_\beta(L)}{L^2}\int \frac{d^2l_1}{(2\pi)^2}F_\alpha(\vec{l}_1, \vec{l}_2)[F_\beta(\vec{l}_1, \vec{l}_2)C_{l_1}^{XY,\rm t}C_{l_2}^{X'Y',\rm t} + F_\beta(\vec{l}_2, \vec{l}_1)C_{l_1}^{XY',\rm t}C_{l_2}^{X'Y,\rm t}], \quad \text{(A10)}$$

with $\beta = (YY')$.

TABLE V. The lensing and CIP response functions in the flat-sky limit.

| $XX'$ | $f_{XX'}(\vec{l}_1,\vec{l}_2)$ | $h_{XX'}(\vec{l}_1,\vec{l}_2)$ |
|---|---|---|
| TT | $\tilde{C}_{l_1}^{TT}(\vec{L}\cdot\vec{l}_1)+\tilde{C}_{l_2}^{TT}(\vec{L}\cdot\vec{l}_2)$ | $\tilde{C}_{l_1}^{T,dT}+\tilde{C}_{l_2}^{T,dT}$ |
| TE | $\tilde{C}_{l_1}^{TE}\cos 2\varphi_{\vec{l}_1\vec{l}_2}(\vec{L}\cdot\vec{l}_1)+\tilde{C}_{l_2}^{TE}(\vec{L}\cdot\vec{l}_2)$ | $\tilde{C}_{l_1}^{T,dE}\cos 2\varphi_{\vec{l}_1\vec{l}_2}+\tilde{C}_{l_2}^{E,dT}$ |
| TB | $\tilde{C}_{l_1}^{TE}\sin 2\varphi_{\vec{l}_1\vec{l}_2}(\vec{L}\cdot\vec{l}_1)$ | $\tilde{C}_{l_1}^{T,dE}\sin 2\varphi_{\vec{l}_1\vec{l}_2}$ |
| EE | $[\tilde{C}_{l_1}^{EE}(\vec{L}\cdot\vec{l}_1)+\tilde{C}_{l_2}^{EE}(\vec{L}\cdot\vec{l}_2)]\cos 2\varphi_{\vec{l}_1\vec{l}_2}$ | $[\tilde{C}_{l_1}^{E,dE}+\tilde{C}_{l_2}^{E,dE}]\cos 2\varphi_{\vec{l}_1\vec{l}_2}$ |
| EB | $[\tilde{C}_{l_1}^{EE}(\vec{L}\cdot\vec{l}_1)-\tilde{C}_{l_2}^{BB}(\vec{L}\cdot\vec{l}_2)]\sin 2\varphi_{\vec{l}_1\vec{l}_2}$ | $[\tilde{C}_{l_1}^{E,dE}-\tilde{C}_{l_2}^{B,dB}]\sin 2\varphi_{\vec{l}_1\vec{l}_2}$ |
| BB | $[\tilde{C}_{l_1}^{BB}(\vec{L}\cdot\vec{l}_1)+\tilde{C}_{l_2}^{BB}(\vec{L}\cdot\vec{l}_2)]\cos 2\varphi_{\vec{l}_1\vec{l}_2}$ | $[\tilde{C}_{l_1}^{B,dB}+\tilde{C}_{l_2}^{B,dB}]\cos 2\varphi_{\vec{l}_1\vec{l}_2}$ |

Finally, we can combine all of these to form a "minimum-variance" estimator [28,41]

$$\hat{d}_{\rm mv}(\vec{L})\equiv\sum_\alpha w_\alpha(L)\hat{d}_\alpha(\vec{L}), \tag{A11}$$

where the weights $w_\alpha$ are chosen to minimize the Gaussian noise,

$$w_\alpha(L)\equiv\frac{\sum_\beta(\mathbf{N}^{-1})_{\alpha\beta}}{\sum_{\beta\gamma}(\mathbf{N}^{-1})_{\beta\gamma}}. \tag{A12}$$

We can now write a minimum-variance estimator for the lensing-potential power spectrum,

$$\hat{C}_L^{\phi\phi}\equiv\frac{1}{2\pi}\int_0^{2\pi}\frac{\hat{d}_{\rm mv}(\vec{L})\hat{d}^*_{\rm mv}(\vec{L})}{L^2}d\varphi_{\vec{L}}-B(L), \tag{A13}$$

where $\varphi_{\vec{L}}$ is the angular coordinate of $\vec{L}$ and $B(L)$ is the standard Gaussian and non-Gaussian biases to the full four-point correlation [29,39,40]. Using Eq. (A6), it is straightforward to show that in the presence of CIPs the bias-subtracted lensing-potential power-spectrum estimator has an expectation value [28,40]

$$\langle\hat{C}_L^{\phi\phi}\rangle=C_L^{\phi\phi}+C_L^{\Delta\Delta}\sum_{\alpha,\beta}w_\alpha(L)w_\beta(L)Q_\alpha(L)Q_\beta(L), \tag{A14}$$

where

$$Q_\alpha(L)\equiv\frac{\int\frac{d^2l_1}{(2\pi)^2}[h_{XX'}(\vec{l}_1,\vec{l}_2)+h_{X'X}(\vec{l}_1,\vec{l}_2)]F_{XX'}(\vec{l}_1,\vec{l}_2)}{\int\frac{d^2l_1}{(2\pi)^2}[f_{XX'}(\vec{l}_1,\vec{l}_2)+f_{X'X}(\vec{l}_1,\vec{l}_2)]F_{XX'}(\vec{l}_1,\vec{l}_2)}, \tag{A15}$$

where the CIP response functions, $h_{XX'}$, are given in Table V. Note that we have left off the non-Gaussian and residual CIP Gaussian bias from this expression. As shown in Sec. III, given the current upper limits to $A_{\rm CIP}$, these terms make a negligible contribution to the expectation value of the temperature-only estimator. In addition to this, Ref. [40] demonstrates that the contribution to these biases from correlations other than $TT$ are of about the same order of magnitude and do not change significantly with an improvement in the instrumental noise.

## APPENDIX B: FULL-SKY EXPRESSIONS

The *Planck* CMB lensing analysis in Ref. [29] used the full-sky estimators derived in Ref. [28] to compute the lensing-potential power spectrum. In this appendix we compute the dominant CIP contribution to that estimator.

Consider an ensemble of CMB fields modulated by both a fixed deflection field $\phi$ and a fixed CIP field $\Delta$. These second-order effects produce an off-diagonal covariance [21,22,28],

TABLE VI. The lensing and CIP response functions. "Even" and "odd" indicate that the functions are nonzero only when $L+l+l'$ is even or odd, respectively. To translate from the conventions of Ref. [18], we need to swap $l\leftrightarrow l'$, which leads to a minus sign for the two odd responses, $EB$ and $TB$. Note that the B-mode autocorrelation, BB, vanishes at linear order in the CIP field.

| XX′ | $f_{lL l'}^{XX'}$ | $h_{lL l'}^{XX'}$ | $l+l'+L$ |
|---|---|---|---|
| TT | $\tilde{C}_l^{TT}{}_0G_{l'Ll}+\tilde{C}_{l'}^{TT}{}_0G_{lLl'}$ | $(\tilde{C}_l^{T,dT}+\tilde{C}_{l'}^{T,dT})_0H_{lLl'}$ | even |
| TE | $\tilde{C}_l^{TE}{}_2G_{l'Ll}+\tilde{C}_{l'}^{TE}{}_0G_{lLl'}$ | $\tilde{C}_l^{T,dE}{}_2H_{lLl'}+\tilde{C}_{l'}^{E,dT}{}_0H_{lLl'}$ | even |
| TB | $i\tilde{C}_l^{TE}{}_2G_{l'Ll}$ | $i\tilde{C}_l^{T,dE}{}_2H_{lLl'}$ | odd |
| EE | $\tilde{C}_l^{EE}{}_2G_{l'Ll}+\tilde{C}_{l'}^{EE}{}_2G_{lLl'}$ | $(\tilde{C}_l^{E,dE}+\tilde{C}_{l'}^{E,dE})_2H_{lLl'}$ | even |
| EB | $i[\tilde{C}_l^{EE}{}_2G_{l'Ll}-\tilde{C}_{l'}^{BB}{}_2G_{lLl'}]$ | $i(\tilde{C}_l^{E,dE}+\tilde{C}_{l'}^{B,dB})_2H_{lLl'}$ | odd |
| BB | $\tilde{C}_l^{BB}{}_2G_{l'Ll}+\tilde{C}_{l'}^{BB}{}_2G_{lLl'}$ | $(\tilde{C}_l^{B,dB}+\tilde{C}_{l'}^{B,dB})_2H_{lLl'}$ | even |

$$\langle X_{lm}X'_{l'm'}\rangle|_{\rm lens,CIP} = \tilde{C}_l^{XX'}\delta_{ll'}\delta_{m-m'}(-1)^m + \sum_{LM}(-1)^M \begin{pmatrix} l & l' & L \\ m & m' & -M \end{pmatrix} \times [\phi_{LM} f_{lLl'}^{XX'} + \Delta_{LM} h_{lLl'}^{XX'}], \tag{B1}$$

where $\phi_{LM}$ and $\Delta_{LM}$ are the multipoles of the lensing potential and CIP field, respectively, $f_{lLl'}^{XX'}$ and $h_{lLl'}^{XX'}$ are the lensing/CIP response functions for different quadratic pairs (see Table VI) and are defined in terms of the unmodulated power spectrum, $\tilde{C}_l^{XX'}$, and the lensing angular/CIP response functions

$${}_{\pm s}G_{lLl'} \equiv [L(L+1)+l'(l'+1)-l(l+1)] \times \sqrt{\frac{(2L+1)(2l+1)(2l'+1)}{16\pi}} \begin{pmatrix} l & L & l' \\ \pm s & 0 & \mp s \end{pmatrix}, \tag{B2}$$

$${}_{\pm s}H_{lLl'} \equiv \sqrt{\frac{(2L+1)(2l+1)(2l'+1)}{4\pi}} \begin{pmatrix} l & L & l' \\ \pm s & 0 & \mp s \end{pmatrix}. \tag{B3}$$

We also define the full-sky power spectrum analogous to Eq. (43)

$$C_l^{T,dT} \equiv \frac{2}{\pi}\int k^2 dk P_\Phi(k) T_l(k) \frac{dT_l(k)}{d\Delta}. \tag{B4}$$

*Planck* estimates the lensing-potential from observations of the CMB uses the formalism presented in Ref. [28], which establishes a minimum-variance estimator for $d_{LM} \equiv \sqrt{L(L+1)}\phi_{LM}$,

$$\hat{d}_{LM}^{\alpha} = A_L^{\alpha} \sum_{lm,l'm'} (-1)^M X_{lm} X'_{l'm'} \begin{pmatrix} l & l' & L \\ m & m' & M \end{pmatrix} F_{ll'L}^{\alpha}, \tag{B5}$$

where $A_L^{\alpha}$ and $F_{ll'L}^{\alpha}$ are

$$A_L^{\alpha} = L(L+1)(2L+1)\left\{\sum_{l_1 l_2} g_{l_1 L l_2}^{\alpha} f_{l_1 L l_2}^{\alpha}\right\}^{-1}, \tag{B6}$$

$$F_{lLl'}^{\alpha} \equiv \frac{C_{l'}^{XX,\rm t} C_l^{X'X',\rm t} f_{lLl'}^{\alpha *} - (-1)^{l+L+l'} C_l^{XX',\rm t} C_{l'}^{XX',\rm t} f_{l'Ll}^{\alpha *}}{C_l^{XX,\rm t} C_{l'}^{XX,\rm t} C_l^{X'X',\rm t} C_{l'}^{X'X',\rm t} - (C_l^{XX',\rm t} C_{l'}^{XX',\rm t})^2}, \tag{B7}$$

where $\alpha = XX'$, and yield, in the absence of a CIP modulation, an optimal estimator

$$\hat{C}_L^{\phi\phi} = \frac{1}{2L+1}\sum_{\alpha,\beta}\sum_{M=-L}^{L} w_\alpha w_\beta \frac{\hat{d}_{LM}^{\alpha}\hat{d}_{LM}^{*\beta}}{L(L+1)} - B_L, \tag{B8}$$

where [28]

$$w_\alpha \equiv N_L^{\rm mv}\sum_\beta (\mathbf{N}_L^{-1})^{\alpha\beta}, \tag{B9}$$

$$N_L^{\alpha\beta} \equiv \frac{A_L^{\alpha *} A_L^{\beta}}{L(L+1)(2L+1)}\sum_{l_1 l_2}\{F_{l_1 L l_2}^{\alpha *}[C_{l_1}^{XY,\rm t} C_{l_2}^{X'Y',\rm t} F_{l_1 L l_2}^{\beta} + (-1)^{L+l_1+l_2} C_{l_1}^{XY',\rm t} C_{l_2}^{X'Y,\rm t} F_{l_2 L l_1}^{\beta}]\} \tag{B10}$$

$$N_L^{\rm mv} \equiv \left[\sum\nolimits_{\alpha\beta}(\mathbf{N}_L^{-1})^{\alpha\beta}\right]^{-1} \tag{B11}$$

are weights chosen to yield an optimal estimator for the deflection field and $B_L$ are the standard Gaussian and non-Gaussian contributions to the CMB four-point correlation [29,39,40]. With a nonzero CIP contribution in Eq. (B1), it is straightforward to show that the lensing estimator in Eq. (B8) becomes biased with an expectation value

$$\langle \hat{C}_L^{\phi\phi}\rangle = C_L^{\phi\phi} + \sum_{\alpha,\beta} w_\alpha w_\beta Q_L^{\alpha} Q_L^{\beta} C_L^{\Delta\Delta}, \tag{B12}$$

where

$$Q_L^{\alpha} \equiv \frac{\sum_{ll'} h_{lLl'}^{\alpha} F_{lLl'}^{\alpha}}{\sum_{ll'} f_{lLl'}^{\alpha} F_{lLl'}^{\alpha}}. \tag{B13}$$

## APPENDIX C: COMPUTING THE SECOND-ORDER CIP EFFECTS

We start by noting that in the absence of the CIPs, the power spectrum, $C_l^{\rm XX'}$, can be written in terms of an integral over wave number [59],

$$C_l^{\rm XX'} = \frac{2}{\pi}\int k^2 dk P_\Phi(k) X_l(k) X'_l(k), \tag{C1}$$

where the $X_l(k)$ weighted integrals of the transfer function, $f^X(\eta)$, along the line of sight are

$$X_l(k) \equiv \int d\eta f^X(\eta) j_l[k(\eta_0 - \eta)]. \tag{C2}$$

A CIP causes a modulation of the transfer function, yielding an observed power spectrum [22]

$$C_l^{XX',\mathrm{obs}} \simeq \tilde{C}_l^{XX'}|_{\Delta=0} + \sum_{Ll'} C_L^{\Delta} C_{l'}^{dX,dX'} ({}_{s_X}K_{ll'}^{L})({}_{s_{X'}}K_{ll'}^{L}) G_{Ll'} + \frac{1}{2}\Delta^2_{\mathrm{rms}}(R_{\mathrm{CMB}})(C_l^{X,d^2X'} + C_l^{X',d^2X}), \quad \text{(C3)}$$

where

$$C_l^{dT,dT} \equiv \frac{2}{\pi}\int k^2 dk P_\Phi(k)\left(\frac{dT_l(k)}{d\Delta}\right)^2, \quad \text{(C4)}$$

$$C_l^{T,d^2T} \equiv \frac{2}{\pi}\int k^2 dk P_\Phi(k) T_l(k)\frac{d^2T_l(k)}{d\Delta^2}, \quad \text{(C5)}$$

$$G_{L,l'} \equiv \frac{(2L+1)(2l'+1)}{4\pi}, \quad \text{(C6)}$$

$${}_{s_X}K_{ll'}^{L} \equiv \begin{pmatrix} l & L & l' \\ s_X & 0 & -s_X \end{pmatrix}, \quad \text{(C7)}$$

and $s_X = 0$ for $X = T$ and $s_X = 2$ for $X = E, B$.

Throughout this work we have taken the CIP modulation to be scale-invariant so that $C_L^{\Delta} \propto L^{-2}$. This means that the terms in the sum of Eq. (C10) will be dominated by smaller values of $L$. Since the variation of the baryon density mainly affects the physics at the surface of last scattering and earlier, the $C_{l'}^{dX,dX'}$ term is only significant on scales smaller than the angular scale of the horizon at decoupling (so $l' \gtrsim 100$); this means that within the sum the terms which dominate have $L \ll l'$. The Wigner 3-j symbol in ${}_sK_{ll'}^{L}$ is only nonzero when $l$, $L$, and $l'$ satisfy the triangle inequality as follows:

$$|l - L| \le l' \le l + L. \quad \text{(C8)}$$

This set of inequalities applies to the three sides of a triangle. If $l'$ and $L$ are two sides of a triangle, given that $l' \gg L$, the only way to complete it is to add another side with $l \simeq l'$. This is the case, and it is straightforward to show that the summand in Eq. (C3) peaks at $l' = l$ and that we have

$$\sum_{l'} ({}_{s_X}K_{ll'}^{L})({}_{s_{X'}}K_{ll'}^{L}) \simeq \frac{1}{2l'+1}\delta_{l,l'}. \quad \text{(C9)}$$

Therefore, we have

$$\sum_{Ll'} C_L^{\Delta} C_{l'}^{dX,dX'} ({}_{s_X}K_{ll'}^{L})({}_{s_{X'}}K_{ll'}^{L}) G_{Ll'} \simeq C_l^{dX,dX'} \sum_L \frac{2L+1}{4\pi} C_L^{\Delta} = \Delta^2_{\mathrm{rms}}(R_{\mathrm{CMB}}) C_l^{dX,dX'}. \quad \text{(C10)}$$

Equation (C1) tells us that the second derivative of the *power spectrum* with respect to $\Delta$ can be written as

$$\frac{1}{2}\frac{d^2C_l^{XX'}}{d\Delta^2} = \frac{2}{\pi}\int k^2 dk P_\Phi(k)\left[\left(\frac{dX_l(k)}{d\Delta}\right)^2 + \frac{1}{2}\left(X_l'(k)\frac{d^2X_l(k)}{d\Delta^2} + X_l(k)\frac{d^2X_l'(k)}{d\Delta^2}\right)\right]. \quad \text{(C11)}$$

This shows that in the presence of a scale-invariant CIP power spectrum the full calculation of the $C_l$s in Eq. (C3) can be replaced with the less computationally intensive expression

$$C_l^{\mathrm{XX'},\mathrm{obs}} \simeq \tilde{C}_l^{\mathrm{XX'}} + \frac{1}{2}\Delta^2_{\mathrm{rms}}(R_{\mathrm{CMB}})\left.\frac{d^2C_l^{\mathrm{XX'}}}{d\Delta^2}\right|_{\Delta=0}. \quad \text{(C12)}$$

When computing the observed $C_l$s in our MCMC, we use an efficient double-sided derivative to numerically calculate the CIP effects. We detail the accuracy of our numerical derivatives in Appendix D. Note that if the CIP spectrum had a blue tilt, or additional power at small scales, the above equation for the observed power spectrum would no longer be a good approximation.

## APPENDIX D: EFFICIENT COMPUTATION OF THE SECOND-ORDER EFFECTS OF CIPS ON THE CMB POWER SPECTRUM

Given the number of evaluations of the power spectrum during an MCMC analysis, it is essential to use a computationally efficient method to compute the CIP effects on the CMB power spectrum. As shown in Eqs. (38) and (C12) in the flat-sky approximation and with the full sky, respectively, the CIP-modulated CMB power spectrum can be computed by taking the second derivative of the unmodulated power spectrum with respect to the CIP field $\Delta$. As discussed in Sec. II, the CIP field is a spatial modulation of the baryon fraction, so this is equivalent to taking the second derivative of the unmodulated CMB power spectrum with respect to $\Omega_b$. In this appendix we outline the numerical techniques we developed to efficiently and accurately compute this derivative.

We compute the numerical derivative of the power spectrum using the finite difference as follows:

$$\frac{\partial^2 C_l}{\partial\Delta^2} = \frac{C_l[\Delta+\epsilon] - 2C_l[\Delta] + C_l[\Delta-\epsilon]}{\epsilon^2}. \quad \text{(D1)}$$

In order to determine the value of $\epsilon$ which yields the most accurate derivative, we compared Eq. (D1) to the second derivative computed from a densely sampled polynomial fit to $C_l(\Delta)$. In particular, we generated 100 evenly spaced samples $C_l(\Delta)$ within a range of $-.25 < \Delta < .25$ and fit a sixth-order polynomial. We found that increasing the number of samples and polynomial order beyond these values lead to less than a 0.1% change in the second-order derivative across the entire range of $2 \le l \le 5000$.

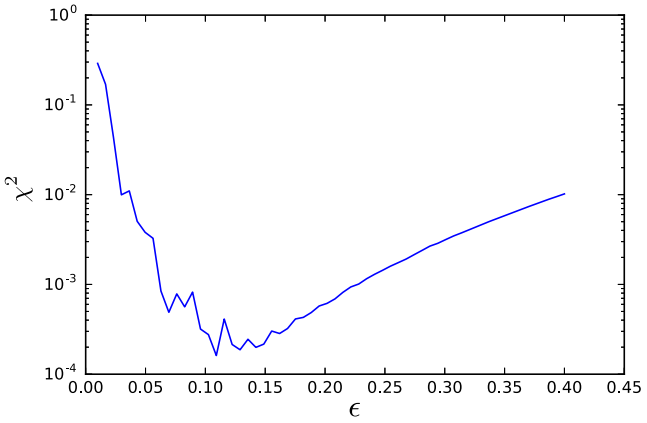


FIG. 10. The fractional difference between the polynomial derivative method and the finite difference [Eq. (D1)] plotted as a function of the step size $\epsilon$ for $C_l^{TT}$ at $\Delta = 0$.

Figure 10 demonstrates the effect of the size of the step size $\epsilon$ in the finite difference formula on how closely this approximation approaches the polynomial-fitting derivative method as quantified by computing the fractional difference, $\chi^2$, between the finite difference and polynomial-fit derivatives,

$$\chi^2 \equiv \frac{\sum_l (y_l - f_l)^2}{\sum_l (y_l)^2}, \tag{D2}$$

where $f_l$ are the finite difference second derivatives of $C_l^{TT}$ and $y_l$ are the polynomial-fit second derivatives. For the accuracy level that we used (in particular, we used AccuracyBoost=1 in CAMB), we can see that the percent difference between our finite difference and polynomial-fit derivatives achieves a minimum of less than 0.1% in the range from $.1 \lesssim \epsilon \lesssim .15$. In the calculations of the CIP-modulated CMB power spectrum we used a step size $\epsilon = 0.1$.

## APPENDIX E: MINIMUM-VARIANCE CIP ESTIMATOR

The CIP field $\Delta_{LM}$ induces off-diagonal correlations between CMB multipoles, as shown in Table VI (and derived in Refs. [18,22]). As with lensing, these correlations can be used to derive a minimum-variance estimator for CIPs, which for a single pair of observables $(X, X' \in \{\mathrm{T}, \mathrm{E}, \mathrm{B}\})$ is

$$\hat{\Delta}^{XX'}_{LM} = N^{XX'}_L \sum_{lml'm'} X_{lm} X'_{l'm'} F^{XX',\mathrm{CIP}}_{lLl'} (-1)^M \times \sqrt{\frac{(2L+1)(2l+1)(2l'+1)}{4\pi}} \begin{pmatrix} l & l' & L \\ m & m' & M \end{pmatrix}, \tag{E1}$$

$$[N^{XX'}_L]^{-1} = \sum_{ll'} G_{ll'} h^{\mathrm{XX}'}_{lLl'} F^{\mathrm{XX}',\mathrm{CIP}}_{lLl'}, \tag{E2}$$

$$G_{ll'} \equiv \frac{(2l+1)(2l'+1)}{4\pi}, \tag{E3}$$

where the filters $F^{XX',\mathrm{CIP}}_{lLl'}$ are as given in Eq. (B7), but using the CIP response functions $h^{\mathrm{XX}'}_{lLl'}$ given in the second column of Table VI in place of the lensing response functions $f^{\mathrm{XX}}_{lLl'}$.

The (Gaussian) reconstruction noise is then

$$\langle |\hat{\Delta}^{XX'}_{LM} - \Delta_{LM}|^2 \rangle_{\mathrm{CMB}} = N^{XX'}_L. \tag{E4}$$

Using different observable pairs, one can obtain the combined total minimum-variance estimator

$$\hat{\Delta}_{LM} = \sum_\alpha w^\alpha_L \hat{\Delta}^\alpha_{LM}, \tag{E5}$$

$$w^\alpha_L = N^{\Delta\Delta}_L \sum_\beta (\mathcal{M}^{-1}_L)^{\alpha,\beta}, \tag{E6}$$

$$[N^{\Delta\Delta}_L]^{-1} \equiv \sum_{\alpha\beta} (\mathcal{M}^{-1}_L)^{\alpha,\beta}. \tag{E7}$$

The estimator covariance-matrix $\mathcal{M}_L$ is at every $L$ a rank-two tensor over observable pairs. The indices $\alpha$ and $\beta$ take values over labels for pairs of observables, that is, $\alpha, \beta \in \{TT, EE, TE, TB, EB\}$. Using Eq. (E1), and identities of Wigner coefficients, we obtain an expression for the matrix elements $\mathcal{M}^{\alpha,\beta}_L$ as follows:

$$\mathcal{M}^{XX',ZZ'}_L = N^{XX'}_L N^{ZZ'}_L \sum_{ll'} G_{ll'} g^{XX'}_{Lll'} \left[ C^{XZ,\mathrm{t}}_{l'} C^{X'Z',\mathrm{t}}_{l} g^{X'Z'*}_{Lll'} + (-1)^{l+l'+L} C^{XZ',\mathrm{t}}_{l'} C^{X'Z,\mathrm{t}}_{l} g^{ZZ'*}_{Ll'l} \right]. \tag{E8}$$

The total-estimator variance is again the inverse normalization factor $N^{\Delta\Delta}_L$.

[1] R. A. Alpher, H. Bethe, and G. Gamow, Phys. Rev. **73**, 803 (1948).
[2] R. H. Cyburt, B. D. Fields, K. A. Olive, and T.-H. Yeh, Rev. Mod. Phys. **88**, 015004 (2016).
[3] R. R. Caldwell and A. Stebbins, Phys. Rev. Lett. **100**, 191302 (2008).
[4] C. Clarkson, B. Bassett, and T. H. -C. Lu, Phys. Rev. Lett. **101**, 011301 (2008).
[5] G. F. Smoot*et al.*, Astrophys. J. Lett. **396**, L1 (1992).
[6] C. L. Bennett, D. Larson, J. L. Weiland, N. Jarosik, G. Hinshaw, N. Odegard, K. M. Smith, R. S. Hill, B. Gold, M. Halpern, E. Komatsu, M. R. Nolta, L. Page, D. N. Spergel, E. Wollack, J. Dunkley, A. Kogut, M. Limon, S. S. Meyer, G. S. Tucker, and E. L. Wright, Astrophys. J. Suppl. Ser. **208**, 20 (2013).
[7] N. Aghanim *et al.* (Planck Collaboration), Astron. Astrophys. **594**, A11 (2016).
[8] P. A. R. Ade *et al.* (Planck Collaboration), Astron. Astrophys. **594**, A17 (2016).
[9] S. Alam *et al.* (BOSS Collaboration), arXiv:1607.03155.
[10] R. Bean, J. Dunkley, and E. Pierpaoli, Phys. Rev. D **74**, 063503 (2006).
[11] P. A. R. Ade *et al.* (Planck Collaboration), Astron. Astrophys. **594**, A20 (2016).
[12] J. L. Bernal, L. Verde, and A. G. Riess, J. Cosmol. Astropart. Phys. 10 (2016) 019.
[13] L. Dai, D. Jeong, M. Kamionkowski, and J. Chluba, Phys. Rev. D **87**, 123005 (2013).
[14] N. MacCrann, J. Zuntz, S. Bridle, B. Jain, and M. R. Becker, Mon. Not. R. Astron. Soc. **451**, 2877 (2015).
[15] R. Adam *et al.* (Planck Collaboration), Astron. Astrophys. **594**, A1 (2016).
[16] A. D. Linde and V. F. Mukhanov, Phys. Rev. D **56**, R535 (1997).
[17] D. H. Lyth, C. Ungarelli, and D. Wands, Phys. Rev. D **67**, 023503 (2003).
[18] C. He, D. Grin, and W. Hu, Phys. Rev. D **92**, 063018 (2015).
[19] T. L. Smith and D. Grin, Phys. Rev. D **94**, 103517 (2016).
[20] C. Gordon and J. R. Pritchard, Phys. Rev. D **80**, 063535 (2009).
[21] D. Grin, O. Doré, and M. Kamionkowski, Phys. Rev. Lett. **107**, 261301 (2011).
[22] D. Grin, O. Doré, and M. Kamionkowski, Phys. Rev. D **84**, 123003 (2011).
[23] G. P. Holder, K. M. Nollett, and A. van Engelen, Astrophys. J. **716**, 907 (2010).
[24] M. T. Soumagnac, R. Barkana, C. G. Sabiu, A. Loeb, A. J. Ross, F. B. Abdalla, S. T. Balan, and O. Lahav, Phys. Rev. Lett. **116**, 201302 (2016).
[25] A. Lewis and A. Challinor, Phys. Rep. **429**, 1 (2006).
[26] J. B. Muñoz, D. Grin, L. Dai, M. Kamionkowski, and E. D. Kovetz, Phys. Rev. D **93**, 043008 (2016).
[27] J. Valiviita, J. Cosmol. Astropart. Phys. 04 (2017) 014.
[28] T. Okamoto and W. Hu, Phys. Rev. D **67**, 083002 (2003).
[29] P. A. R. Ade *et al.* (Planck Collaboration), Astron. Astrophys. **594**, A15 (2016).
[30] M. Bucher, K. Moodley, and N. Turok, Phys. Rev. D **62**, 083508 (2000).
[31] J. R. Bond and G. Efstathiou, Astrophys. J. **285**, L45 (1984).
[32] H. Kodama and M. Sasaki, Int. J. Mod. Phys. A **02**, 491 (1987).
[33] M. Bucher, K. Moodley, and N. Turok, Phys. Rev. D **66**, 023528 (2002).
[34] D. Grin, D. Hanson, G. P. Holder, O. Doré, and M. Kamionkowski, Phys. Rev. D **89**, 023006 (2014).
[35] K. N. Abazajian *et al.* (CMB-S4 Collaboration), arXiv: 1610.02743.
[36] M. Zaldarriaga and U. Seljak, Phys. Rev. D **59**, 123507 (1999).
[37] W. Hu, Phys. Rev. D **62**, 043007 (2000).
[38] A. Lewis and A. Challinor, Phys. Rep. **429**, 1 (2006).
[39] S. Das*et al.*, Phys. Rev. Lett. **107**, 021301 (2011).
[40] M. Kesden, A. Cooray, and M. Kamionkowski, Phys. Rev. D **67**, 123507 (2003).
[41] W. Hu and T. Okamoto, Astrophys. J. **574**, 566 (2002).
[42] R. Adam *et al.* (Planck Collaboration), Astron. Astrophys. **594**, A8 (2016).
[43] A. Lewis and S. Bridle, Phys. Rev. D **66**, 103511 (2002).
[44] K. N. Abazajian *et al.* (CMB-S4 Collaboration), arXiv: 1610.02743.
[45] K. M. Smith, D. Hanson, M. LoVerde, C. M. Hirata, and O. Zahn, J. Cosmol. Astropart. Phys. 06 (2012) 014.
[46] G. Jungman, M. Kamionkowski, A. Kosowsky, and D. N. Spergel, Phys. Rev. D **54**, 1332 (1996).
[47] M. Kamionkowski, A. Kosowsky, and A. Stebbins, Phys. Rev. D **55**, 7368 (1997).
[48] U. Seljak and M. Zaldarriaga, Phys. Rev. Lett. **78**, 2054 (1997).
[49] M. Zaldarriaga and U. Seljak, Phys. Rev. D **55**, 1830 (1997).
[50] W. L. K. Wu, J. Errard, C. Dvorkin, C. L. Kuo, A. T. Lee, P. McDonald, A. Slosar, and O. Zahn, Astrophys. J. **788**, 138 (2014).
[51] R. Flauger, J. C. Hill, and D. N. Spergel, J. Cosmol. Astropart. Phys. 08 (2014) 039.
[52] C. H. Heinrich, D. Grin, and W. Hu, Phys. Rev. D **94**, 043534 (2016).
[53] M. Su, A. P. S. Yadav, M. McQuinn, J. Yoo, and M. Zaldarriaga, arXiv:1106.4313.
[54] K. M. Smith *et al.*, AIP Conf. Proc. **1141**, 121 (2009).
[55] P. Larsen, A. Challinor, B. D. Sherwin, and D. Mak, Phys. Rev. Lett. **117**, 151102 (2016).
[56] V. Gluscevic, M. Kamionkowski, and D. Hanson, Phys. Rev. D **87**, 047303 (2013).
[57] K. Sigurdson, A. Kurylov, and M. Kamionkowski, Phys. Rev. D **68**, 103509 (2003).
[58] J. A. King, J. K. Webb, M. T. Murphy, V. V. Flambaum, R. F. Carswell, M. B. Bainbridge, M. R. Wilczynska, and F. E. Koch, Mon. Not. R. Astron. Soc. **422**, 3370 (2012).
[59] U. Seljak and M. Zaldarriaga, Astrophys. J. **469**, 437 (1996).